JOURNAL OF PETROLOGY | VOLUME 47 | NUMBER 2 | PAGES 385–408 | 2006 | doi:10.1093/petrology/egi079

Calculated Phase Relations in the System NCKFMASH (Na_2O–CaO–K_2O–FeO–MgO–Al_2O_3–SiO_2–H_2O) for High-Pressure Metapelites

CHUNJING WEI[1]* AND ROGER POWELL[2]

[1]MOE KEY LABORATORY OF OROGENIC BELTS AND CRUSTAL EVOLUTION, SCHOOL OF EARTH AND SPACE SCIENCES, PEKING UNIVERSITY, BEIJING 100871, P.R. CHINA

[2]SCHOOL OF EARTH SCIENCES, UNIVERSITY OF MELBOURNE, MELBOURNE, VIC. 3010, AUSTRALIA

RECEIVED APRIL 1, 2005; ACCEPTED SEPTEMBER 21, 2005
ADVANCE ACCESS PUBLICATION OCTOBER 21, 2005

Petrogenetic grids in the system NCKFMASH (Na_2O–CaO–K_2O–FeO–MgO–Al_2O_3–SiO_2–H_2O) and the subsystems NCKMASH and NCKFASH calculated with the software THERMOCALC 3.1 are presented for the P–T *range 7–30 kbar and 450–680°C, for assemblages involving garnet, chloritoid, biotite, carpholite, talc, chlorite, kyanite, staurolite, paragonite, glaucophane, jadeite, omphacite, diopsidic pyroxene, plagioclase, zoisite and lawsonite, with phengite, quartz/coesite and H_2O in excess. These grids, together with calculated compatibility diagrams and* P–T *and* T–X_{Ca} *and* P–X_{Ca} *pseudosections for different bulk-rock compositions, show that incorporation of Ca into the NKFMASH system leads to many of the NKFMASH invariant equilibria moving to lower pressure and/or lower temperature, which results, in most cases, in the stability of jadeite and garnet being enlarged, but in the reduction of stability of glaucophane, plagioclase and AFM phases. The effect of Ca on the stability of paragonite is dependent on mineral assemblage at different* P–T *conditions. The calculated NCKFMASH diagrams are powerful in delineating the phase equilibria and* P–T *conditions of natural pelitic assemblages. Moreover, contours of the calculated phengite Si isopleths in* P–T *and* P–X_{Ca} *pseudosections confirm that phengite barometry in NCKFMASH is strongly dependent on mineral assemblage.*

KEY WORDS: *phase relations; metapelites; NCKFMASH; THERMOCALC; phengite geobarometry*

INTRODUCTION

On the basis of internally consistent thermodynamic datasets (Holland & Powell, 1990, 1998), a number of quantitative petrogenetic grids for various model systems have been constructed in the last decade and a half (Guiraud *et al.*, 1990; Powell & Holland, 1990; Xu *et al.*, 1994; Mahar *et al.*, 1997; Will *et al.*, 1998; Carson *et al.*, 1999; White *et al.*, 2001; Wei & Powell, 2003, 2004; Wei *et al.*, 2003). These petrogenetic grids contain all the pressure–temperature–composition (*P–T–X*) information for mineral assemblages in a model system, which can be applied through sections and pseudosections by variously fixing pressure, temperature or bulk-rock composition (Powell *et al.*, 1998). In principle, such calculations allow phase diagrams to be constructed that closely approximate the phase relations in natural rocks.

Since characteristic high-pressure (HP) and ultrahigh-pressure (UHP) parageneses such as kyanite + talc, talc + phengite and pyrope + coesite in metapelites were first reported (Kulke & Schreyer, 1973; Abraham & Schreyer, 1976; Chopin, 1981, 1984), studies on the phase relations in HP and UHP metapelites have been carried out via both laboratory experiments (Schreyer, 1977, 1988; Chopin & Schreyer, 1983; Massonne & Schreyer, 1989; Massonne, 1995, 2000; Hermann, 2002) and thermodynamic modeling (Guiraud *et al.*, 1990; Will *et al.*, 1998; Proyer, 2003; Wei & Powell, 2003, 2004). For example,

*Corresponding author. Telephone: 86-10-62754157. Fax: 86-10-62751159. E-mail: cjwei@pku.edu.cn

© The Author 2005. Published by Oxford University Press. All rights reserved. For Permissions, please e-mail: journals.permissions@oxfordjournals.org

Downloaded from http://petrology.oxfordjournals.org/ at Indiana University School of Medicine Libraries on September 22, 2012

Wei & Powell (2003) presented a petrogenetic grid for KFMASH with mineral phases garnet, chloritoid, carpholite, talc, chlorite, staurolite, phengite, biotite, kyanite/sillimanite, quartz/coesite and H_2O, including the compositional variations in the solid solutions involving the $FeMg_{-1}$ and the Tschermak's $(Fe, Mg)_{-1}Si_{-1}Al^{VI}Al^{IV}$ exchange vectors, thus extending the previous simple equilibria in KMASH to Fe-bearing HP mineral assemblages. Most obviously, incorporation of Fe into the KMASH system favors the stability of chloritoid and garnet. With incorporation of Na_2O and the relevant Na phases albite, paragonite, glaucophane and jadeite, Wei & Powell (2004) extended this KFMASH grid, showing that addition of Na_2O leads to more complicated phase relations in the NKFMASH system. However, Na_2O does not change the basic phase relations because the Na is mostly present in independent Na-phases except in its minor substitution via NaK_{-1} in phengite.

It is obvious that natural metapelites also always contain CaO. The incorporation of Ca into minerals involves several types of substitution such as the $Ca(Fe,Mg)_{-1}$ in garnet, $Ca(Fe, Mg)Na_{-1}Al^{VI}_{-1}$ in glaucophane, jadeite, omphacite and diopsidic pyroxene, and $CaAl^{IV}Na_{-1}Si_{-1}$ in paragonite and plagioclase. For example, the glaucophane phengite schist documented by Wei & Powell (2004) from the Chinese southern Tianshan HP–LT belt contains a mineral assemblage garnet + glaucophane + phengite + albite + quartz with a small amount of CaO present mainly in garnet. If the CaO content is higher, the independent Ca-phases such as zoisite and lawsonite are commonly present. These zoisite- and lawsonite-bearing metapelites and felsic rocks are extensive in HP–UHP terranes around the world (Oberhänsli *et al.*, 1985; Koons, 1986; El-Shazly & Liou, 1991; Compagnoni & Rolfo, 2000; Liu *et al.*, 2001; Okay, 2002). A good example, considered further below, is the metagranite from the Sesia–Lanzo Zone in Italy, which contains an assemblage of quartz + omphacite/jadeite + garnet + white mica + zoisite (Oberhänsli *et al.*, 1985). How this incorporation of CaO affects the NKFMASH phase relations needs to be examined. In addition, Wei & Powell (2003, 2004) have extended the experimentally calibrated phengite geobarometer (Massonne & Schreyer, 1987, 1989; Massonne & Szpurzka, 1997) to various KFMASH and NKFMASH parageneses: the applicability of this geobarometric method to NCKFMASH assemblages also requires further development.

In this paper, petrogenetic grids in the model system NCKFMASH and the subsystems NCKMASH and NCKFASH are presented in the P–T range 7–30 kbar and 450–680°C. To consider the mineral equilibria in metapelitic rocks, combinations of garnet, chloritoid, carpholite, talc, chlorite, staurolite, biotite, paragonite, glaucophane, jadeite, omphacite, diopsidic pyroxene, plagioclase, kyanite/sillimanite, zoisite and lawsonite with phengite, quartz/coesite and H_2O in excess are involved in the grids presented. From a general point of view the omission of Ca-rich amphiboles is inappropriate, even though they are uncommon in metapelites, because a large part of the P–T–X space of interest does involve them. However, casual inspection of the projections presented here reveals that they are already full of lines, and if the Ca-rich amphiboles were to be added to the projections, they would become impossible to read. Conversely, NCKFMASH for metabasic rocks has to be constructed including these minerals, and in this case carpholite, chloritoid, etc. would be omitted to make the results readable. One way adopted here to focus on the part of composition space that the calculated mineral equilibria are appropriate for is to use a compatibility diagram that addresses the part of composition space of interest and puts out of view parts for which it is inappropriate.

In constructing these grids, we adopted the internally consistent dataset of Holland & Powell (1998) and subsequent upgrades in 2001, the software THERMOCALC 3.1 (Powell *et al.*, 1998) and updated models of activity–composition relationships for solid solutions. Ideal mixing models are used for talc and carpholite, symmetric mixing models for garnet, chloritoid and staurolite, the asymmetric formalism model for phengite, Darken's quadratic formalism (DQF, Powell, 1987) for glaucophane, plagioclase and paragonite, and symmetric order–disorder models for ordered chlorite, biotite, jadeite, omphacite and diopsidic pyroxene. (For details see the Appendix.)

PETROGENETIC GRIDS

The calculated P–T projections in the P–T range 7–30 kbar and 450–680°C of interest for the subsystems NCKMASH and NCKFASH and the full system NCKFMASH are presented in Figs 1, 2 and 3a, and calculated results for the invariant points are tabulated in Tables 1–3.

NCKMASH grid

In the subsystem NCKMASH (Fig. 1), there are 22 invariant equilibria stable in the P–T range of interest involving the above phases exclusive of garnet, chloritoid and staurolite. Invariant equilibrium m2 does not involve K_2O, Na_2O and CaO, so it, and the four univariant reactions emanating from it, are the same as those in the KMASH and NKMASH grids (Wei & Powell, 2003, 2004). These reactions constrain the maximum stabilities of chlorite and Mg-carpholite and also the lower P–T limits of the typical white schist paragenesis kyanite + talc. Relative to the corresponding invariant equilibria in NKMASH, the three invariant equilibria

Downloaded from http://petrology.oxfordjournals.org/ at Indiana University School of Medicine Libraries on September 22, 2012

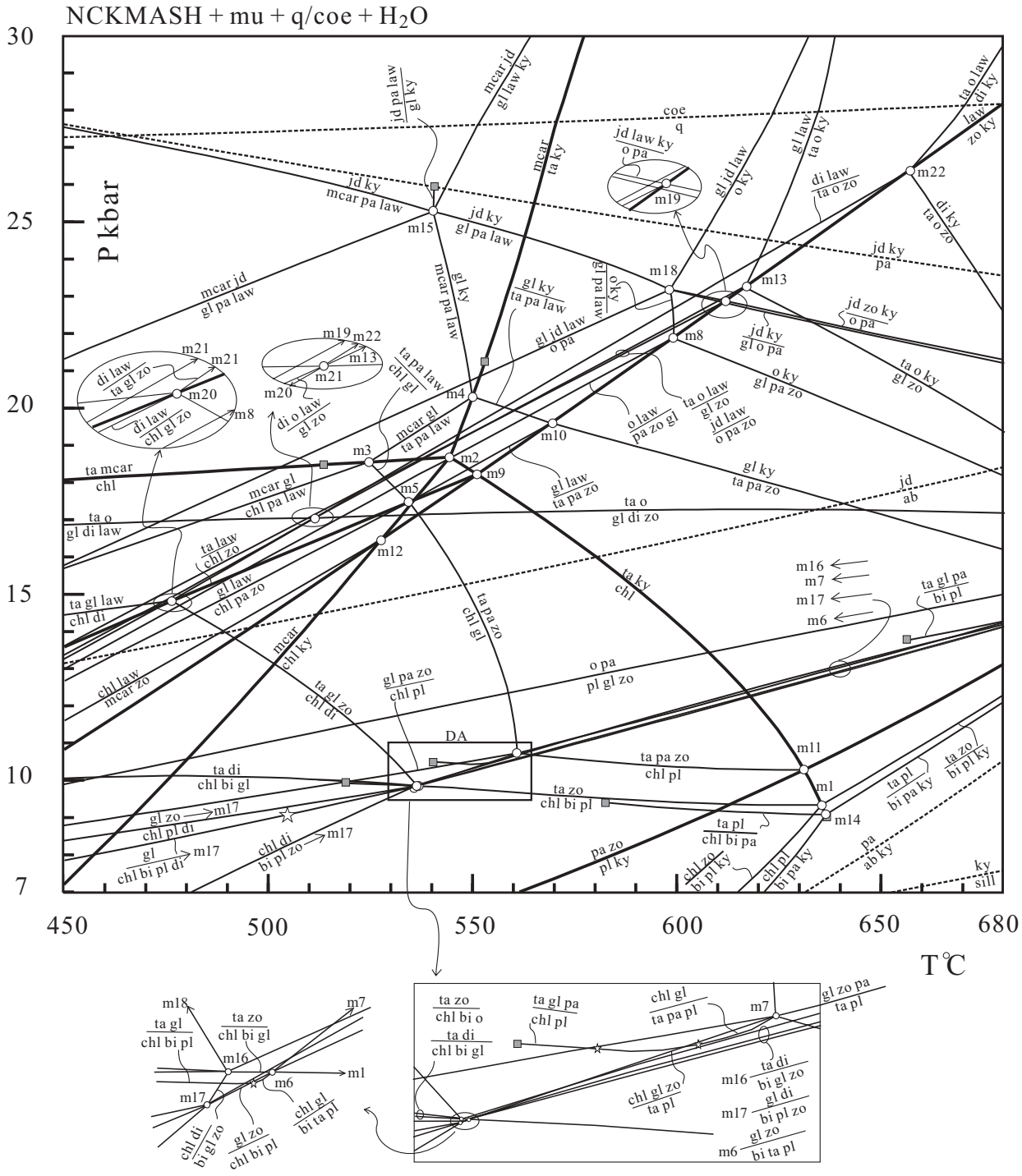

Fig. 1. *P–T* projection for the subsystem NCKMASH in projection from phengitic muscovite, quartz/coesite and H_2O. Open circles with labels m1–m22 refer to the invariant points in NCKMASH and grey squares refer to the invariant points in NKMASH. For clarity, reactions that are stable across invariant points are shown as bold lines. Open stars indicate the location of singularities, and the phases that change sides of the reaction are shown in italics. The reactions coe = q, pa + q = jd + ky, pa + q = ab + ky, jd + q = ab and ky = sill are shown as dashed lines. DA shows details around invariant points m6, m7, m16 and m17. Mineral abbreviations: ab, albite; bi, biotite; chl, chlorite; coe, coesite; di, diopsidic pyroxene, gl, glaucophane; jd, jadeite; ky, kyanite; law, lawsonite; mcar, Mg-carpholite; o, omphacite; pa, paragonite; mu, phengitic muscovite; pl, plagioclase; q, quartz; ta, talc; sill, sillimanite; zo, zoisite.

Downloaded from http://petrology.oxfordjournals.org/ at Indiana University School of Medicine Libraries on September 22, 2012

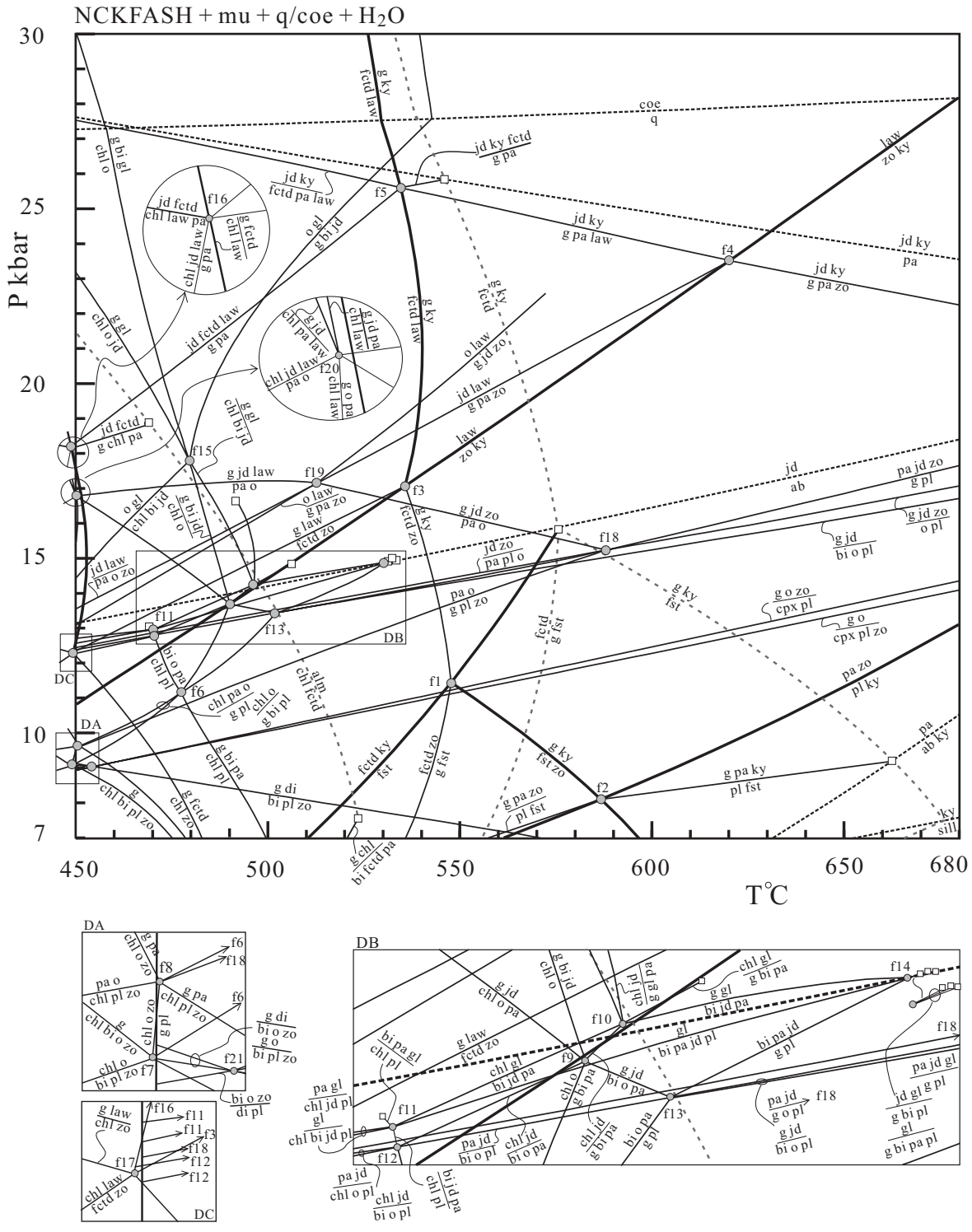

Fig. 2. *P–T* projection for the subsystem NCKFASH in projection from phengitic muscovite, quartz/coesite and H_2O. Grey circles with labels f1–f21 refer to the invariant points in NCKFASH and open squares refer to the invariant points in NKFASH. For comparison, (NK)FMASH reactions showing the low-*T* limit of almandine, and the high-*T* limits of Fe-chloritoid and Fe-staurolite are shown as grey dashed lines. Reactions that are stable across invariant points are shown as bold lines. Open stars indicate the location of singularities, and the phases that change sides of the reaction are shown in italics. DA shows details around invariant points f7 and f8; DB shows details around invariant points f9–f14; DC shows details around invariant point f17. Mineral abbreviations: alm, almandine; fctd, Fe-chloritoid; fst, Fe-staurolite, g, garnet. Other abbreviations are as in Fig. 1.

Downloaded from http://petrology.oxfordjournals.org/ at Indiana University School of Medicine Libraries on September 22, 2012

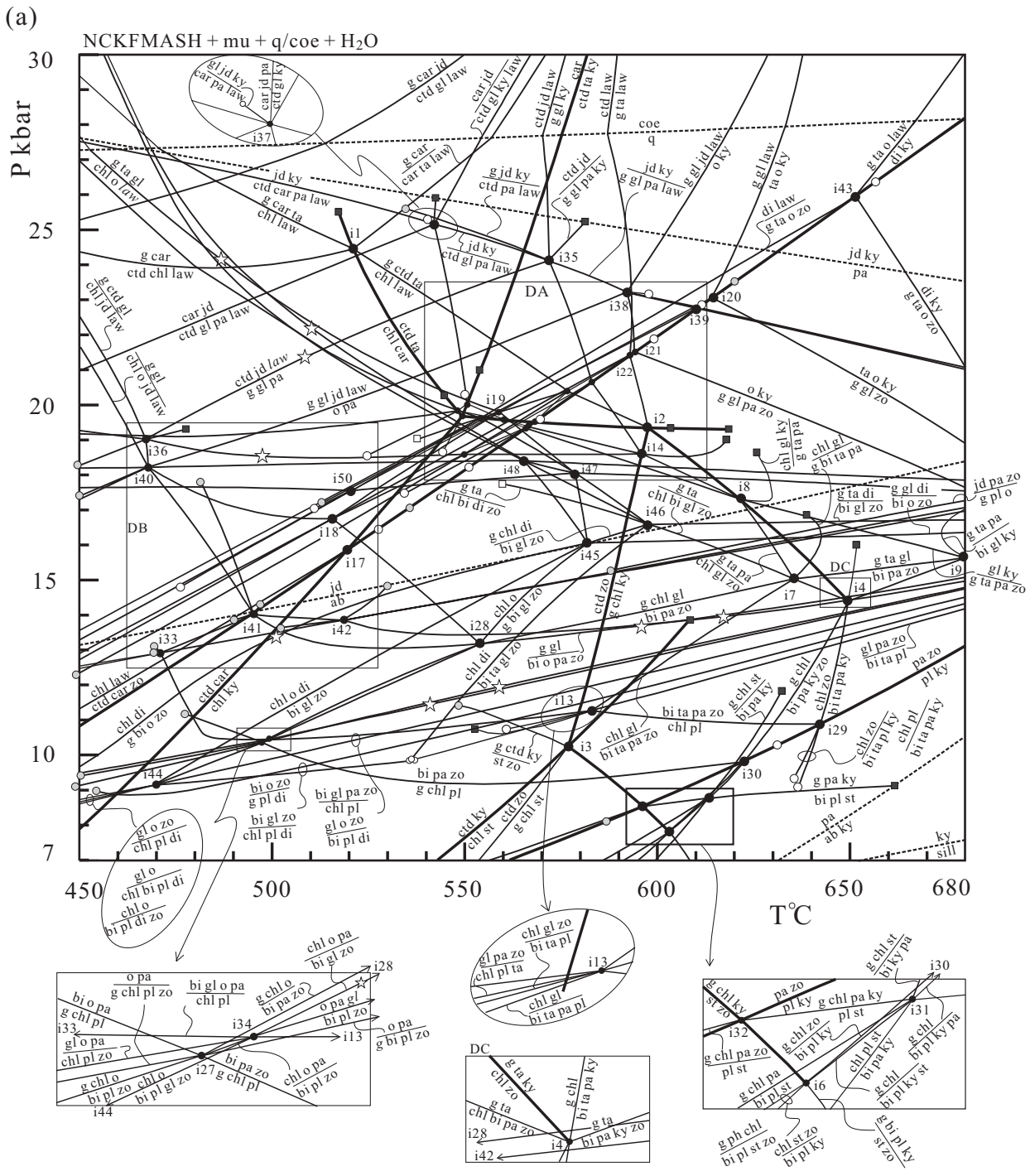

Fig. 3. (a) *P–T* projection for the full system NCKFMASH in projection from phengitic muscovite, quartz/coesite and H_2O. Filled circles with label i1–i50 refer to the invariant points in NCKFMASH. Full system reactions terminating at subsystem invariant points are shown by open circles for NCKMASH, light grey circles for NCKFASH, filled squares for NKFMASH and open squares for CKFMASH, respectively, with the subsystem reactions omitted for clarity. Bold lines represent the univariant reactions that are stable across invariant points. Open stars indicate the location of singularities, and the phases that change sides of the reaction are shown in italics. DA and DB: details of the equilibria are shown in (b) and (c); DC: details of the equilibria around invariant point i4. Mineral abbreviations: car, carpholite; ctd, chloritoid; st, staurolite. Other abbreviations are as in Figs 1 and 2. (b) Details of the equilibria in the rectangle DA in (a). (c) Details of the equilibria in the rectangle DB in (a).

Downloaded from http://petrology.oxfordjournals.org/ at Indiana University School of Medicine Libraries on September 22, 2012

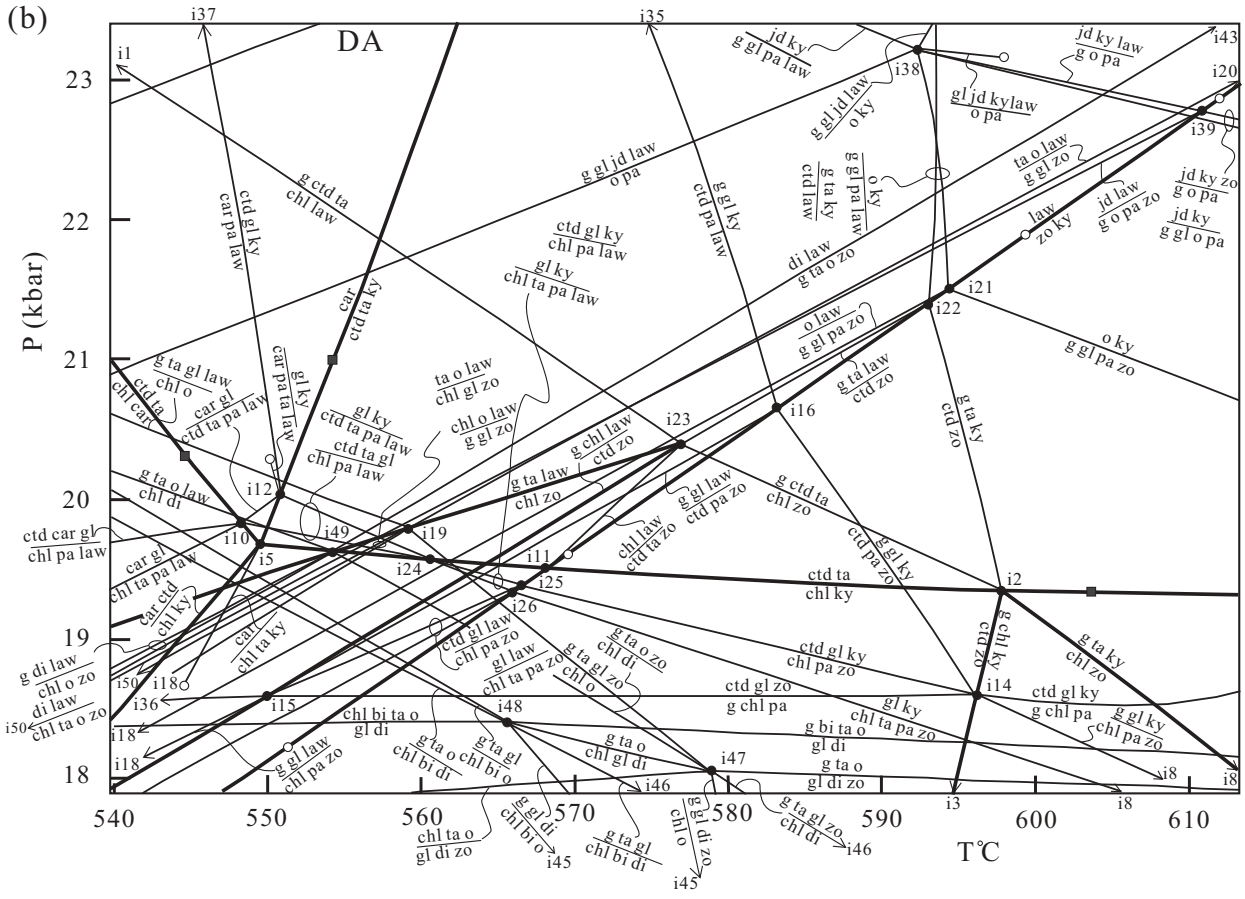

Fig. 3. Continued.

m4 and m15, with pressures above m2, shift to lower pressure by <1 kbar, and the three invariant equilibria m3, m6 and m7, with pressures below m2, move to higher temperatures by 10–20°C. The univariant reactions emanating from these five invariant points show similar slopes and phase topologies to those in NKMASH. The other invariant equilibria are particular to NCKMASH.

With incorporation of Ca, the stability fields of glaucophane, paragonite and plagioclase are reduced. For example, the high-*P* limit of NKMASH glaucophane is restricted by the reaction ky + gl = ta + jd corresponding to the classical NMASH reaction gl + coe = ta + jd of Holland (1988) at over 34–36 kbar, whereas NCKMASH glaucophane would be consumed through reaction m13(law) gl + zo = ta + o + ky at pressures below 23 kbar if zoisite is present, and through reaction m13(zo) gl + law = ta + o + ky at temperatures above 620–640°C. [The notation 'name (phase)' means reaction 'phase'-out emanating from invariant point 'name' (see Tables 1–3 for the *P*–*T* coordinates of the invariant points).] The low-*P* limit of the paragenesis kyanite + jadeite is given by three paragonite-involving reactions m15(gl) mcar + pa + law = jd + ky, m18(o) gl + pa + law = jd + ky and m18(law) gl + o + pa = jd + ky, at a lower pressure than the NASH reaction pa + q = jd + ky, the pressure difference increasing as temperature increases. In relation to kyanite eclogites, the coexistence of omphacite and kyanite is constrained by reactions m8(law) gl + pa + zo = o + ky, m8(zo) gl + pa + law = o + ky and m18(pa) gl + jd + law = o + ky, with *P*–*T* conditions above 18 kbar and 600°C. This is analogous to the conditions calculated by Carson *et al.* (1999) and Wei *et al.* (2003), and also consistent with the estimated *P*–*T* conditions of >600°C and >20 kbar for kyanite-bearing eclogite from natural occurrences and experimental studies (Holland, 1979, 1988). As temperature rises to ~660°C, the paragenesis diopsidic pyroxene + kyanite becomes stable.

NCKFASH grid

The calculated *P*–*T* projection for NCKFASH is shown in Fig. 2 and the calculated results for the stable invariant equilibria are listed in Table 2. There are 21 stable invariant equilibria involving phases garnet, chlorite,

Downloaded from http://petrology.oxfordjournals.org/ at Indiana University School of Medicine Libraries on September 22, 2012

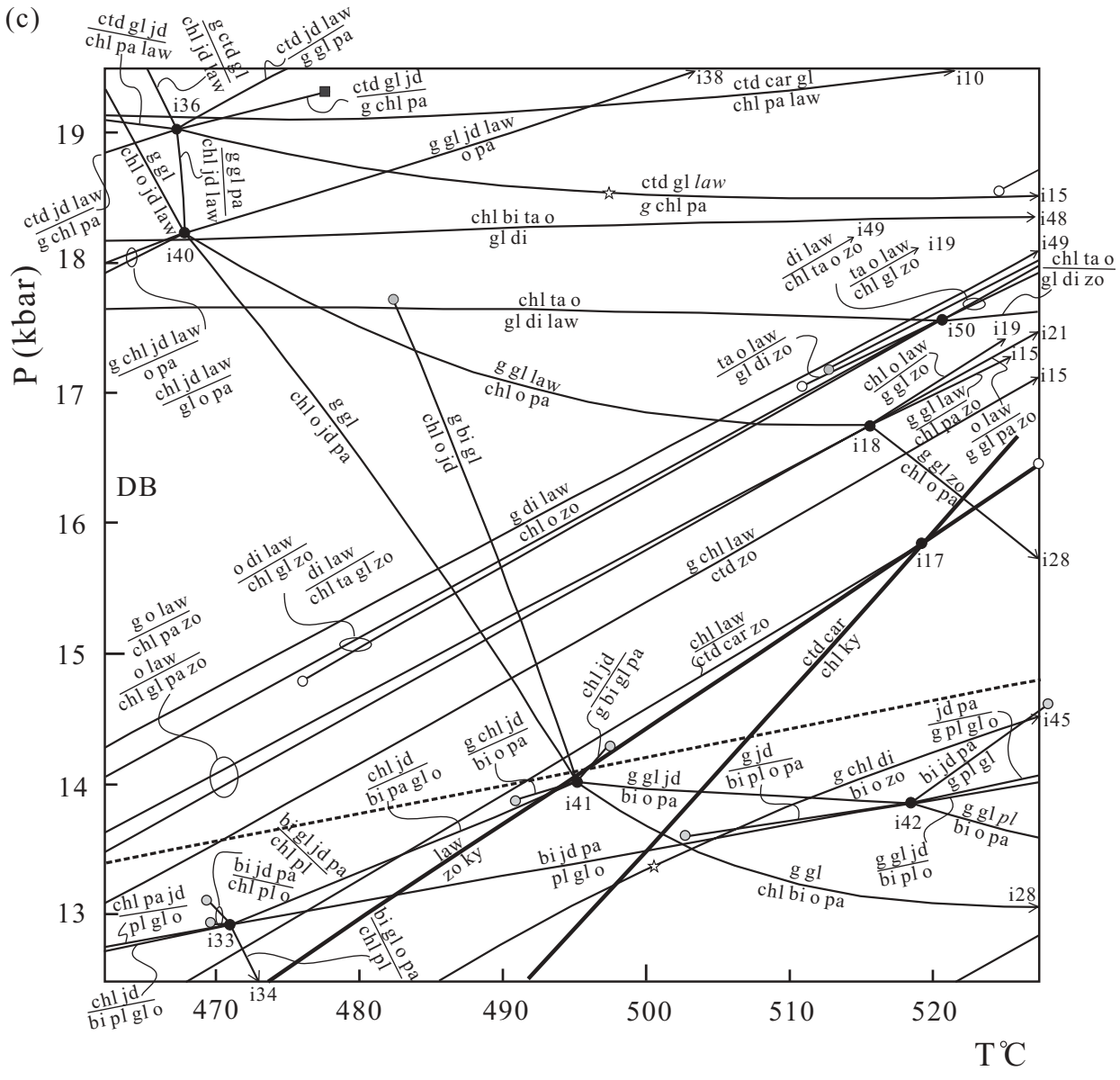

Fig. 3. Continued.

Fe-chloritoid, Fe-staurolite, biotite, glaucophane, paragonite, plagioclase, jadeite, omphacite, diopsidic pyroxene, kyanite, lawsonite and zoisite (+ phengite + quartz/coesite + H_2O). The NCKFASH grid in Fig. 2 differs significantly from the NKFASH grid of Wei & Powell (2004). Relative to the corresponding invariant equilibria in NKFASH, the three invariant points f1, f2 and f5 move to lower temperatures by 10–70°C and to lower pressures by 1–4 kbar, reducing the stabilities of Fe-chloritoid and Fe-staurolite to lower temperatures, in the presence of a Ca-phase, zoisite or lawsonite. With incorporation of Ca, the stability field of garnet extends to lower temperatures than does almandine in NKFASH (Wei & Powell, 2004). If phengite is in excess, the low-T limit of garnet in Fig. 2 is provided by reactions f7(o) chl + bi + pl + zo = g and f7(pl) chl + bi + o + zo = g, and if phengite is absent, garnet is stable to much lower temperatures.

With addition of CaO, the stability field of jadeite-bearing assemblages is enlarged relative to those in NKFASH. For example, the paragenesis jadeite + kyanite in the NCKFASH subsystem is constrained by reactions f4(law) g + pa + zo = jd + ky, f4(zo) g + pa + law = jd + ky and f5(g) fctd + pa + law = jd + ky, and is

Downloaded from http://petrology.oxfordjournals.org/ at Indiana University School of Medicine Libraries on September 22, 2012

Table 1: Calculated results for the invariant equilibria in the subsystem NCKMASH

	Phases (+ mu + q + H_2O)	*P* (kbar)	*T* (°C)	y(mu)	z(mu)	y(bi)	y(chl)	N(chl)	y(ta)	J(jd)	N(jd)	J(o)	N(o)	J(di)	N(di)	c(pl)	N(gl)	c(pa)
m1	chl, bi, ta, pl, zo, ky	9·34	635·5	0·90	0·05	0·35	0·55	0·45	0·09							0·53		
m2	chl, ta, pa, mcar, law, ky	18·68	544·4	0·79	0·03		0·52	0·48	0·04									0·03
m3	chl, ta, gl, pa, mcar, law	18·55	524·6	0·75	0·02		0·51	0·49	0·03								0·93	0·02
m4	ta, gl, pa, mcar, law, ky	20·30	550·0	0·75	0·03				0·04								0·93	0·02
m5	chl, ta, gl, pa, law, zo	17·47	534·5	0·76	0·03		0·51	0·49	0·04								0·92	0·03
m6	chl, bi, ta, pl, gl, zo	9·86	536·6	0·76	0·03	0·10	0·51	0·49	0·04							0·15	0·87	
m7	chl, ta, pl, gl, pa, zo	10·73	561·0	0·81	0·05		0·51	0·49	0·05							0·16	0·88	0·05
m8	gl, o, pa, law, zo, ky	21·88	599·0	0·75	0·03							0·53	0·39				0·92	0·03
m9	chl, ta, pa, law, zo, ky	18·22	551·1	0·79	0·03		0·52	0·48	0·04									0·04
m10	ta, gl, pa, law, zo, ky	19·59	569·2	0·76	0·03				0·04								0·91	0·04
m11	chl, ta, pl, pa, zo, ky	10·28	631·1	0·90	0·08		0·54	0·46	0·09							0·40		0·15
m12	chl, pa, mcar, law, zo, ky	16·47	527·7	0·85	0·04		0·54	0·48										0·06
m13	ta, gl, o, law, zo, ky	23·24	616·6	0·67	0·02				0·04			0·48	0·38				0·89	
m14	chl, bi, ta, pl, pa, ky	9·08	636·5	0·92	0·11	0·36	0·55	0·45	0·09							0·23		0·07
m15	gl, jd, pa, mcar, law, ky	25·28	540·3	0·70	0·02					0·94	0·01						0·97	0·00
m16	chl, bi, ta, gl, di, zo	9·86	536·2	0·76	0·03	0·10	0·51	0·49	0·04					0·10	0·01		0·87	
m17	chl, bi, pl, gl, di, zo	9·84	535·8	0·76	0·03	0·10	0·51	0·49						0·10	0·01	0·15	0·87	
m18	gl, o, pa, jd, law, ky	23·18	598·2	0·73	0·03					0·82	0·04	0·58	0·35				0·94	0·02
m19	o, pa, jd, law, zo, ky	22·87	611·9	0·78	0·03					0·81	0·04	0·58	0·34					0·02
m20	chl, ta, gl, di, law, zo	14·81	476·2	0·61	0·01		0·50	0·49	0·02					0·10	0·01		0·90	
m21	ta, gl, o, di, law, zo	17·03	511·3	0·61	0·01				0·02			0·45	0·40	0·12	0·02		0·89	
m22	ta, o, di, law, zo, ky	26·36	656·6	0·60	0·01				0·04			0·40	0·30	0·22	0·06			

$y(mu) = x_{Al}^{M2A}$, $N(mu) = Na/(K + Na)$, $y(bi) = x_{Al}^{M1}$, $y(chl) = x_{Al}^{T2}$, $N(chl) = (x_{Al}^{M4} - x_{Al}^{M1})/2$, $y(ta) = x_{Al}^{M3}$, $J(jd, o, di) = Al^{M1}/(Al + Mg)^{M1}$, $N(jd, o, di) = (x_{Al}^{M1b} - x_{Al}^{M1a})/2$, $c(pl) = Ca/(Ca + Na)$, $N(gl) = [Na/(Na + Ca)]^{M4}$ and $c(pa) = Ca/(Na + Ca)$.

stable at lower pressures than the NASH reaction pa + q = jd + ky, as in NCKMASH. The parageneses paragonite + jadeite constrained by a series of reactions emanating from invariant points f12, f13 and f18 is about 1–2 kbar lower than the maximum stability boundary provided by the NAS reaction jd + q = ab. The parageneses omphacite + kyanite and diopsidic pyroxene + kyanite are not stable in the NCKFASH grid, suggesting that these assemblages in natural occurrences are favored by more magnesian bulk-rock compositions. The stabilities of paragonite, Fe-glaucophane and plagioclase are reduced with addition of CaO, as in NCKMASH.

NCKFMASH grid

The full system NCKFMASH grid is shown in Fig. 3a and the calculated results for the stable invariant equilibria are listed in Table 3. There are 50 invariant points stable in the *P*–*T* range of interest with combinations of the phases garnet, biotite, chlorite, chloritoid, talc, carpholite, staurolite, glaucophane, kyanite, paragonite, plagioclase, jadeite, omphacite, diopsidic pyroxene, lawsonite and zoisite (+ phengitic muscovite + quartz/coesite + H_2O). The stable NCKMASH and NCKFASH univariant equilibria of Figs 1 and 2 and the NKFMASH univariant equilibria presented by Wei & Powell (2004) are not presented for clarity. Like those in the NCKMASH and NCKFASH subsystems, most invariant points in the full NCKFMASH system move to lower pressures and temperatures by about 0·5–3·5 kbar and 0–30°C relative to the corresponding invariant points in the NKFMASH subsystem, the moves becoming more significant at lower pressure and higher temperature conditions. In comparison with the NKFMASH grid of Wei & Powell (2004), the incorporation of Ca tends to enlarge the stability fields of jadeite and garnet, but reduce the stabilities of paragonite, glaucophane, plagioclase and many AFM phases such as chlorite, chloritoid, staurolite, talc and biotite.

The full system grid, even with the omission of the calcic amphiboles, is complex and hard to read. This type of *P*–*T* grid, although giving the general maximum stability limits of minerals and mineral assemblages, is

Downloaded from http://petrology.oxfordjournals.org/ at Indiana University School of Medicine Libraries on September 22, 2012

Table 2: Calculated results of the invariant equilibria in the subsystem NCKFASH

	Phases (+ mu + q + H_2O)	*P* (kbar)	*T* (°C)	z(g)	y(mu)	z(mu)	y(bi)	y(chl)	N(chl)	J(jd)	N(jd)	J(o)	N(o)	N(di)	J(di)	N(gl)	c(pa)	c(pl)
f1	g, pa, fctd, fst, zo, ky	11·45	547·7	0·24	0·96	0·07										0·13		
f2	g, pa, pl, fst, zo, ky	8·10	586·7	0·24	0·97	0·10											0·20	0·52
f3	g, pa, fctd, law, zo, ky	17·07	535·7	0·28	0·93	0·05											0·05	
f4	g, pa, jd, law, zo, ky	23·51	620·1	0·37	0·88	0·04				0·91	0·02						0·02	
f5	g, pa, jd, fctd, law, ky	25·61	534·5	0·10	0·81	0·02				0·96	0·00						0·00	
f6	g, chl, bi, pa, o, pl	11·16	477·4	0·32	0·70	0·02	0·11	0·51	0·48			0·50	0·43				0·01	0·03
f7	g, chl, bi, o, pl, zo	9·08	449·3	0·51	0·73	0·02	0·12	0·51	0·48			0·46	0·42					0·06
f8	g, chl, pa, o, pl, zo	9·65	450·8	0·49	0·75	0·02		0·51	0·48			0·48	0·44				0·01	0·06
f9	g, chl, bi, pa, o, jd	13·71	490·1	0·17	0·61	0·02	0·08	0·51	0·48	0·86	0·00	0·55	0·41				0·00	
f10	g, chl, bi, pa, jd, gl	14·25	496·4	0·10	0·60	0·02	0·08	0·51	0·48	0·91	0·00						0·00	
f11	chl, bi, pa, jd, gl, pl	12·96	470·5		0·59	0·01	0·06	0·51	0·48	0·90	0·00					0·99	0·00	0·01
f12	chl, bi, pa, o, jd, pl	12·85	470·9		0·60	0·01	0·07	0·51	0·48	0·87	0·00	0·55	0·41				0·00	0·01
f13	g, bi, pa, o, jd, pl	13·45	502·0	0·17	0·62	0·02	0·09			0·86	0·00	0·55	0·40				0·00	0·01
f14	g, bi, pa, jd, gl, pl	14·91	530·0	0·01	0·59	0·02	0·09			0·99	0·00					0·99	0·00	0·01
f15	g, chl, bi, o, jd, gl	17·79	479·6	0·12	0·36	0·00	0·02	0·50	0·49	0·87	0·00	0·55	0·41			0·98		
f16	g, chl, pa, jd, fctd, law	18·18	448·5	0·17	0·61	0·01		0·51	0·48	0·92	0·00						0·00	
f17	g, chl, pa, fctd, law, zo	12·30	449·3	0·37	0·83	0·03		0·52	0·47								0·02	
f18	g, pa, o, jd, pl, zo	15·24	588·1	0·46	0·82	0·05				0·80	0·00	0·57	0·35				0·02	0·06
f19	g, pa, o, jd, law, zo	17·17	512·8	0·47	0·77	0·03				0·85	0·00	0·56	0·39				0·01	
f20	g, chl, pa, o, jd, law	16·79	450·1	0·24	0·61	0·01		0·51	0·48	0·89	0·00	0·54	0·42				0·00	
f21	g, bi, o, di, pl, zo	9·05	454·5	0·53	0·73	0·01	0·12					0·46	0·42	0·12	0·00			0·07

z(g) = Ca/(Ca + Fe), J(jd, o, di) = $Al^{M1}/(Al + Fe)^{M1}$, N(jd, o, di) = $(x_{Al}^{M1b} - x_{Al}^{M1a})/2$, and the other composition variables are as in Table 1.

primarily used as the essential information to allow the drawing of compatibility diagrams and pseudosections.

COMPATIBILITY DIAGRAMS

To illustrate the changes in mineral assemblage and the compositions of coexisting minerals with respect to *P*–*T* and bulk-rock composition, a series of calculated compatibility diagrams were drawn, involving projection onto the Al_2O_3–$FeNaAlO_3$–$MgNaAlO_3$ plane from phengitic muscovite, paragonite, zoisite, quartz and H_2O. To simplify the full grid in the context of the projecting phases in the compatibility diagrams, a *P*–*T* projection with phengite, paragonite, zoisite, quartz and H_2O in excess is presented in Fig. 4, including also the relevant univariant reactions in the NCKMASH and NCKFASH subsystems. In the lawsonite stability field in Fig. 4, above the law = zo + ky reaction, lawsonite is considered to be in excess. For clarity, the reactions involving both lawsonite and zoisite are eliminated. In the presence of zoisite and paragonite, biotite is not stable under the *P*–*T* conditions along the chosen traverse (A–L in Fig. 4), limited by a series of reactions such as i27(o) g + chl + pl = bi, i27(pl) g + chl + o = bi, i7(ta) g + chl + gl = bi and i7(chl) g + ta + gl = bi in Fig. 4. Thus, the phase equilibria along the chosen traverse will be similar to those in NCFMASH because only one K-phase, phengitic muscovite, is present (see Fig. 5).

In Fig. 5A, chlorite is a complete solid solution between Fe and Mg end-members and chloritoid is Fe-rich. Different mineral assemblages occur in different metapelitic bulk-rock compositions; for example, the chl–pl paragenesis is stable in Na-rich rocks and ctd–ky is stable in Fe- and Al-rich rocks, whereas in the Mg- and Al-rich rocks, the stable mineral assemblages are ctd–chl–ky and/or chl–ky. At this stage, carpholite has broken down by virtue of the full system reaction i17(law) car + ctd = chl + ky and the NCKMASH subsystem reaction m12(law) mcar = chl + ky. With *P*–*T* increase, the NCKFASH reaction f8(o) chl + pl = g leads to the appearance of Fe–Ca-rich garnet, giving the g–chl–pl divariant triangle in Fe- and Na-rich rocks. The NCKMASH subsystem reaction m7(ta) chl + pl = gl results in the formation of glaucophane in Na- and Mg-rich rocks, and the NCKFASH subsystem reaction chl = g + fctd causes the breakdown of Fe-rich chlorite in Fe-rich rocks, giving rise to the g–chl–ctd divariant triangle in Fig. 5B. From B to C, the NCKFMASH reaction i27(bi) g + chl + pl = o produces omphacite in Na- and Fe-rich rocks (Fig. 5C). Across the full system reaction i34(bi)

Downloaded from http://petrology.oxfordjournals.org/ at Indiana University School of Medicine Libraries on September 22, 2012

Table 3: Calculated results for the invariant equilibria in the system NCKFMASH

	Phases (+ mu + q + H_2O)	*P* (kbar)	*T* (°C)	x(g)	z(g)	x(ctd)	x(mu)	y(mu)	x(chl)	y(chl)	x(bi)	y(bi)	x(st)	x(gl)	N(gl)	x(o)	J(o)	c(pl)
i1	g, ctd, chl, car, ta, gl, law	24·45	521·0	0·73	0·12	0·57	0·29	0·46	0·33	0·51				0·18	0·95			
i2	g, ctd, chl, ta, gl, ky, zo	19·35	597·6	0·50	0·24	0·34	0·17	0·73	0·18	0·52				0·10	0·90			
i3	g, ctd, chl, pa, st, ky, zo	10·25	576·8	0·67	0·22	0·65	0·39	0·91	0·40	0·57			0·83					
i4	g, chl, bi, ta, pa, ky, zo	14·47	649·0	0·46	0·20		0·17	0·82	0·15	0·54	0·19	0·19						
i5	ctd, chl, car, ta, pa, ky, law	19·67	549·3			0·13	0·05	0·75	0·06	0·52								
i6	g, chl, bi, pl, st, ky, zo	7·81	603·2	0·65	0·20		0·35	0·92	0·34	0·58	0·39	0·38	0·79					0·64
i7	g, chl, bi, ta, gl, pa, zo	15·08	635·2	0·48	0·23		0·18	0·79	0·17	0·53	0·21	0·15		0·11	0·87			
i8	g, chl, ta, gl, pa, ky, zo	17·31	621·4	0·48	0·23		0·17	0·77	0·16	0·53				0·10	0·89			
i9	g, bi, ta, gl, pa, ky, zo	15·68	678·6	0·39	0·20		0·14	0·79			0·15	0·19		0·08	0·86			
i10	ctd, chl, car, ta, gl, pa, law	19·83	548·2			0·15	0·06	0·75	0·07	0·52				0·04	0·93			
i11	ctd, chl, ta, gl, ky, zo, law	19·51	568·0			0·22	0·10	0·75	0·10	0·52				0·06	0·91			
i12	ctd, car, ta, gl, pa, ky, law	20·03	550·6			0·14	0·06	0·76						0·03	0·93			
i13	chl, bi, ta, pl, gl, pa, zo	11·27	583·0				0·05	0·81	0·05	0·52	0·07	0·15		0·03	0·87			
i14	g, ctd, chl, gl, pa, ky, zo	18·60	596·0	0·52	0·24	0·37	0·19	0·76	0·19	0·52				0·11	0·91			
i15	g, ctd, chl, gl, pa, zo, law	18·59	549·8	0·58	0·30	0·52	0·27	0·73	0·29	0·52				0·17	0·93			
i16	g, ctd, gl, pa, ky, zo, law	20·64	582·9	0·54	0·27	0·41	0·21	0·73						0·12	0·92			
i17	ctd, chl, car, pa, ky, zo, law	15·84	519·3			0·21	0·08	0·86	0·09	0·53								
i18	g, chl, gl, o, pa, zo, law	16·75	515·6	0·58	0·36		0·38	0·70	0·42	0·51				0·26	0·94	0·39	0·50	
i19	g, chl, ta, gl, o, zo, law	19·80	559·1	0·51	0·35		0·22	0·61	0·23	0·51				0·13	0·89	0·19	0·45	
i20	g, ta, gl, o, ky, zo, law	23·07	614·4	0·44	0·27		0·14	0·65						0·08	0·89	0·11	0·47	
i21	g, gl, o, pa, ky, zo, law	21·51	594·2	0·53	0·28		0·22	0·72						0·13	0·93	0·19	0·52	
i22	g, ctd, ta, gl, ky, zo, law	21·41	592·9	0·49	0·26	0·33	0·16	0·69						0·09	0·90			
i23	g, ctd, chl, ta, gl, zo, law	20·40	576·7	0·52	0·28	0·38	0·18	0·69	0·19	0·52				0·11	0·90			
i24	ctd, chl, ta, gl, pa, ky, law	19·57	560·4			0·19	0·08	0·75	0·09	0·52				0·05	0·92			
i25	ctd, chl, gl, pa, ky, zo, law	19·38	566·4			0·22	0·10	0·75	0·10	0·52				0·06	0·91			
i26	chl, ta, gl, pa, ky, zo, law	19·34	565·8				0·09	0·75	0·09	0·52				0·05	0·91			
i27	g, chl, bi, pl, o, pa, zo	10·36	497·2	0·56	0·43		0·65	0·76	0·68	0·51	0·67	0·07				0·72	0·47	0·08

	Phases (+ mu + q + H_2O)	*P* (kbar)	*T* (°C)	x(g)	z(g)	x(ctd)	x(mu)	y(mu)	x(chl)	y(chl)	x(bi)	y(bi)	x(st)	x(gl)	N(gl)	x(jd)	J(jd)	x(o)	J(o)	c(pl)
i28	g, chl, bi, gl, o, pa, zo	13·17	554·0	0·57	0·36		0·37	0·75	0·39	0·52	0·41	0·07		0·26	0·91			0·38	0·47	
i29	chl, bi, ta, pl, pa, ky, zo	10·89	642·3				0·06	0·89	0·05	0·54	0·07	0·30								0·37
i30	g, chl, bi, pl, pa, ky, zo	9·84	622·7	0·59	0·21		0·28	0·91	0·26	0·56	0·31	0·30								0·42
i31	g, chl, bi, pl, pa, st, ky	8·76	613·1	0·68	0·15		0·34	0·92	0·33	0·57	0·38	0·34	0·78							0·39
i32	g, chl, pl, pa, st, ky, zo	8·54	596·2	0·66	0·21		0·36	0·92	0·35	0·58			0·80							0·50
i33	chl, bi, pl, gl, o, jd, pa	12·93	471·3				0·98	0·60	0·98	0·51	0·98	0·06		0·96	0·99	0·99	0·89	0·99	0·55	
i34	chl, bi, pl, gl, o, pa, zo	10·45	499·1				0·31	0·75	0·33	0·51	0·37	0·05		0·21	0·92			0·32	0·47	0·08
i35	g, ctd, gl, jd, pa, ky, law	24·12	572·0	0·68	0·16	0·54	0·30	0·69						0·18	0·96	0·32	0·88			
i36	g, ctd, chl, gl, jd, pa, law	19·03	467·4	0·81	0·17	0·91	0·72	0·60	0·78	0·51				0·59	0·98	0·78	0·91			
i37	ctd, car, gl, jd, pa, ky, law	25·16	542·1			0·45	0·22	0·68						0·13	0·97	0·24	0·93			
i38	g, gl, o, jd, pa, ky, law	23·23	592·3	0·18	0·23		0·26	0·71						0·15	0·95	0·26	0·82	0·24	0·58	
i39	g, o, jd, pa, ky, zo, law	22·79	610·8	0·11	0·32		0·33	0·76								0·33	0·80	0·31	0·59	
i40	g, chl, gl, o, jd, pa, law	18·23	468·0	0·77	0·21		0·73	0·60	0·79	0·51				0·61	0·98	0·79	0·89	0·79	0·55	
i41	g, chl, bi, gl, o, jd, pa	14·01	495·4	0·86	0·14		0·96	0·60	0·97	0·51	0·97	0·07		0·94	0·99	0·97	0·88	0·98	0·56	
i42	g, bi, pl, gl, o, jd, pa	13·86	518·6	0·85	0·14		0·89	0·62			0·91	0·08		0·83	0·99	0·92	0·86	0·92	0·57	

Downloaded from http://petrology.oxfordjournals.org/ at Indiana University School of Medicine Libraries on September 22, 2012

Table 3: continued

	Phases (+ mu + q + H_2O)	*P* (kbar)	*T* (°C)	x(g)	z(g)	x(ctd)	x(mu)	y(mu)	x(chl)	y(chl)	x(bi)	y(bi)	x(gl)	N(gl)	x(o)	J(o)	x(di)	J(di)	c(pl)
i43	g, ta, o, di, ky, zo, law	25·97	651·6	0·34	0·28		0·10	0·59							0·07	0·40	0·06	0·22	
i44	chl, bi, pl, gl, o, di, zo	9·15	469·6				0·16	0·71	0·18	0·50	0·25	0·04	0·11	0·91	0·16	0·45	0·12	0·10	0·08
i45	g, chl, bi, gl, o, di, zo	16·06	582·1	0·52	0·34		0·25	0·68	0·25	0·51	0·29	0·07	0·16	0·88	0·22	0·42	0·20	0·17	
i46	g, chl, bi, ta, gl, di, zo	16·60	597·8	0·51	0·32		0·21	0·69	0·21	0·51	0·25	0·08	0·13	0·87			0·16	0·17	
i47	g, chl, ta, gl, o, di, zo	18·06	579·0	0·51	0·34		0·22	0·65	0·22	0·51			0·13	0·88	0·19	0·42	0·16	0·17	
i48	g, chl, bi, ta, gl, o, di	18·41	565·6	0·56	0·32		0·26	0·56	0·28	0·51	0·31	0·04	0·16	0·89	0·24	0·43	0·21	0·16	
i49	g, chl, ta, o, di, zo, law	19·63	554·4	0·50	0·38		0·22	0·60	0·24	0·51					0·19	0·43	0·16	0·15	
i50	chl, ta, gl, o, di, zo, law	17·56	520·7				0·13	0·60	0·14	0·51			0·08	0·89	0·11	0·44	0·09	0·13	

x(g) = Fe/(Fe + Mg + Ca), and x(other phases) = Fe/(Fe + Mg); the other composition variables are as in Tables 1 and 2. For clarity, the composition variables N(mu), x(car), x(ta), y(ta), c(pa) and the ordering parameters N(chl, bi, jd, o, di) are neglected.

chl + pl = gl + o, the chl–pl join gives way to o–gl (Fig. 5D). From D to E, the NCKMASH subsystem reaction pl + gl = o leads to the appearance of Mg-rich omphacite in Na- and Mg-rich rocks, and the NCKFASH subsystem reaction f8(chl) g + pl = o produces Fe-rich omphacite in Na- and Fe-rich rocks (Fig. 5E), resulting in omphacite becoming a complete solid solution between Fe and Mg end-members. From E to F, plagioclase becomes unstable as a result of the NAS reaction jd + q = ab. The full system reaction i18(law) chl + o = g + gl causes the chl–o tie-line to give way to g–gl. The NCKFASH reaction f1(fst) fctd = g + ky leads to the breakdown of Fe-chloritoid, giving the divariant triangle g–ctd–ky in Fe- and Al-rich compositions, and the subsystem NCKMASH reaction m5(law) chl + gl = ta produces talc, giving another divariant triangle chl–ta–gl in Mg-rich compositions (Fig. 5F). With *P–T* increase from F to G, the NCKFASH reaction f18(pl) o = g + jd produces the divariant assemblage g–jd–o in Na- and Fe-rich compositions, the NCKMASH subsystem reaction m9(law) chl = ta + ky causes Mg-rich chlorite to break down, and the full system reaction i14(ky) g + chl = ctd + gl leads to the g–chl tie-line being replaced by ctd–gl (Fig. 5G). Across the full system reaction i26(law) chl + ta = gl + ky, the chl–ta join is replaced by gl–ky in Mg-rich compositions (Fig. 5H). From H to I, the full system reaction i14(g) chl = ctd + gl + ky results in the disappearance of chlorite, and the NCKMASH subsystem reaction m10(law) ta = gl + ky leads to the breakdown of talc (Fig. 5I). Across reaction i14(chl) ctd = g + gl + ky, chloritoid breaks down in the system (Fig. 5J). Crossing the full system reaction i21(law) g + gl = o + ky, the g–gl tie-line is replaced by o–ky, producing the kyanite eclogite assemblage in rocks with moderate Fe/(Mg + Fe) (Fig. 5K). With further *P–T* increase, the NCKMASH subsystem reaction m8(law) gl = o + ky leads to the disappearance of glaucophane in Mg-rich rocks, the full system reaction i39(law) g + o = jd + ky causes the g–o tie-line to be replaced by jd–ky, and the NCKMASH subsystem reaction m19(law) o = jd + ky results in the disappearance of omphacite with the phase topology shown in Fig. 5L.

PSEUDOSECTIONS

Phase relations in two samples, from the Tianshan HP belt, NW China, and the Sesia–Lanzo Zone in Italy, are delineated using the NCKFMASH grid in Fig. 3a.

Glaucophane–phengite schist from the southern Tianshan HP belt, NW China

The eclogites and blueschists in the southern Tianshan HP belt, NW China, have been the subject of several recent studies (Gao *et al.*, 1995, 1999; Klemd *et al.*, 2002; Zhang *et al.*, 2002*a*, 2002*b*; Wei *et al.*, 2003; Wei & Powell, 2004). However, the *P–T* conditions of the glaucophane–phengite schist, one of the most extensive rock types in the belt, have not been well determined, nor its relations with the eclogites and blueschists, because of the lack of appropriate geothermobarometers. Wei & Powell (2004) presented a pseudosection in the NKFMASH system for a representative sample (AK07) with a mineral assemblage of garnet + glaucophane + phengite + albite + quartz and obtained *P–T* conditions of about 17–19 kbar and 670–690°C. The pressure was in good agreement with that of a hornblende eclogite in the belt estimated at 17–18 kbar, but the temperature was higher (610–630°C, Wei *et al.*, 2003). A likely reason for this temperature difference is the substitution of CaO in garnet because all the other minerals are effectively CaO-free and lie close to the NKFMASH system. As a result, the phase relations in sample AK07 are re-examined in NCKFMASH. Using the mineral modal proportions and

Downloaded from http://petrology.oxfordjournals.org/ at Indiana University School of Medicine Libraries on September 22, 2012

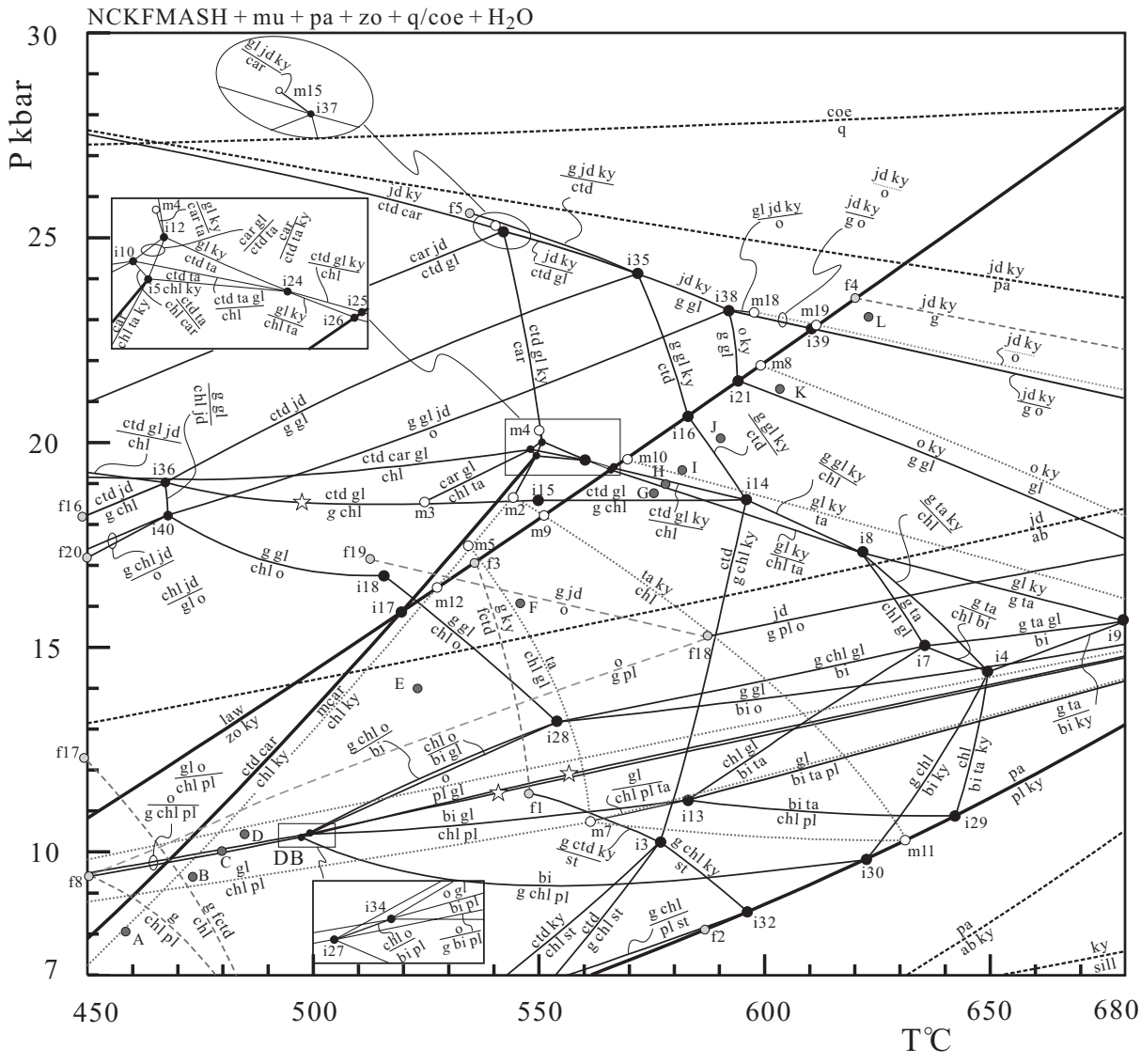

Fig. 4. A simplified*P–T* projection for the full system NCKFMASH in projection from phengitic muscovite, paragonite, zoisite and/or lawsonite, quartz/coesite and H_2O. Dark grey circles with letters A–L are *P–T* locations of the compatibility diagrams shown in Fig. 5. The univariant reactions in the NCKMASH and NCKFASH subsystems relevant to the calculation of the compatibility diagrams along the traverse A–L are shown, respectively, as dotted and dashed lines. (For others see Fig. 3.)

compositions for sample AK07 presented by Wei & Powell (2004), an effective bulk composition was calculated in the NCKFMASH system, giving Al_2O_3:CaO:MgO:FeO:K_2O:Na_2O = 34·79:4·82:13·70:28·15:4·58:13·95 on a mole basis. Using this bulk composition, a *P–T* pseudosection was calculated. For comparison, the *P–T* pseudosection of the NKFMASH grid (Wei & Powell, 2004) was recalculated with the symmetric mixing model for quaternary phengite presented in the Appendix. To keep the internal consistency between the *P–T* and *T*(*P*)–X_{Ca} pseudosections, the bulk composition in the Ca-free system was made in proportion, giving Al_2O_3:MgO:FeO:K_2O:Na_2O = 34·79:14·88:30·58:4·58:15·16. These two pseudosections are presented in Fig. 6a and b. The pseudosection in NCKFMASH (Fig. 6b) is dominated by di-, tri- and quadrivariant fields with one quinivariant field in the high *P–T* region. There are two invariant points i36 and i40 that can be 'seen' by this bulk composition. The corresponding NKFMASH pseudosection in Fig. 6a is dominated by di- and trivariant fields with two quadrivariant fields.

For most mineral assemblages, the two pseudosections can be matched, but the stability fields for garnet and jadeite are enlarged in the Ca-bearing system. Generally, garnet in NCKFMASH appears at a temperature about 30°C lower than in the Ca-free system, depending on

Downloaded from http://petrology.oxfordjournals.org/ at Indiana University School of Medicine Libraries on September 22, 2012

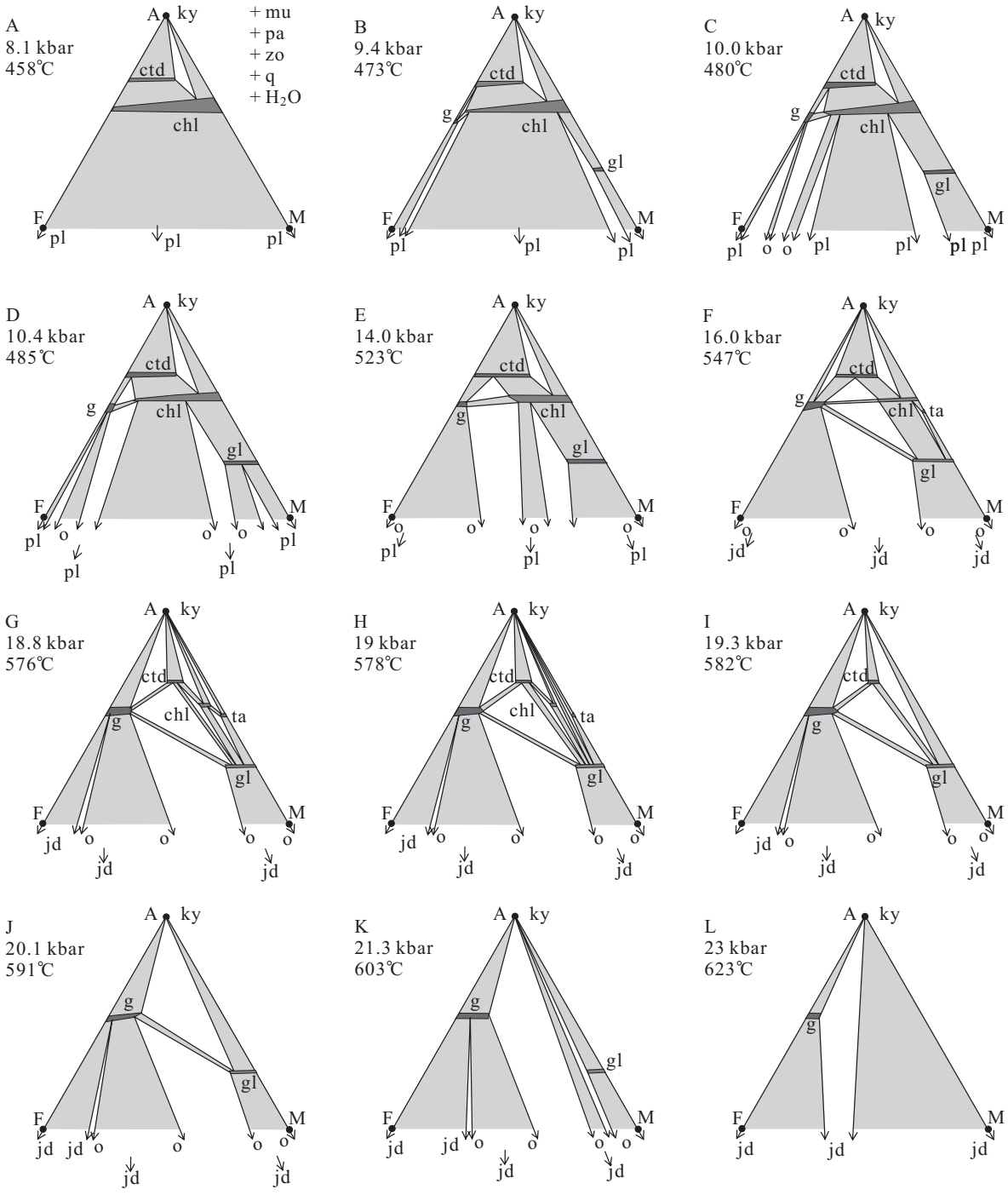

Fig. 5. Al_2O_3–$FeNaAlO_3$–$MgNaAlO_3$ compatibility diagrams, in projection from phengitic muscovite, paragonite, zoisite, quartz and H_2O calculated for the locations A–L in Fig. 4.

pressure and mineral assemblage. This is because plagioclase in the Ca-bearing system plays an important role in garnet stability. The low-*P* limit of jadeite in Fig. 6a is dependent on temperature and mineral assemblage. When the temperature is above ~600°C, jadeite is stable to its maximum stability field and transformed into albite through the NAS reaction jd + q = ab, or through a very narrow divariant field g–mu–gl–jd–ab. When the temperature is below ~600°C, the jadeite-out boundary is mostly controlled by where the mode of jadeite goes to zero. Comparatively, jadeite in Fig. 6b is stabilized to lower pressure by 1–2 kbar and transformed into

Downloaded from http://petrology.oxfordjournals.org/ at Indiana University School of Medicine Libraries on September 22, 2012

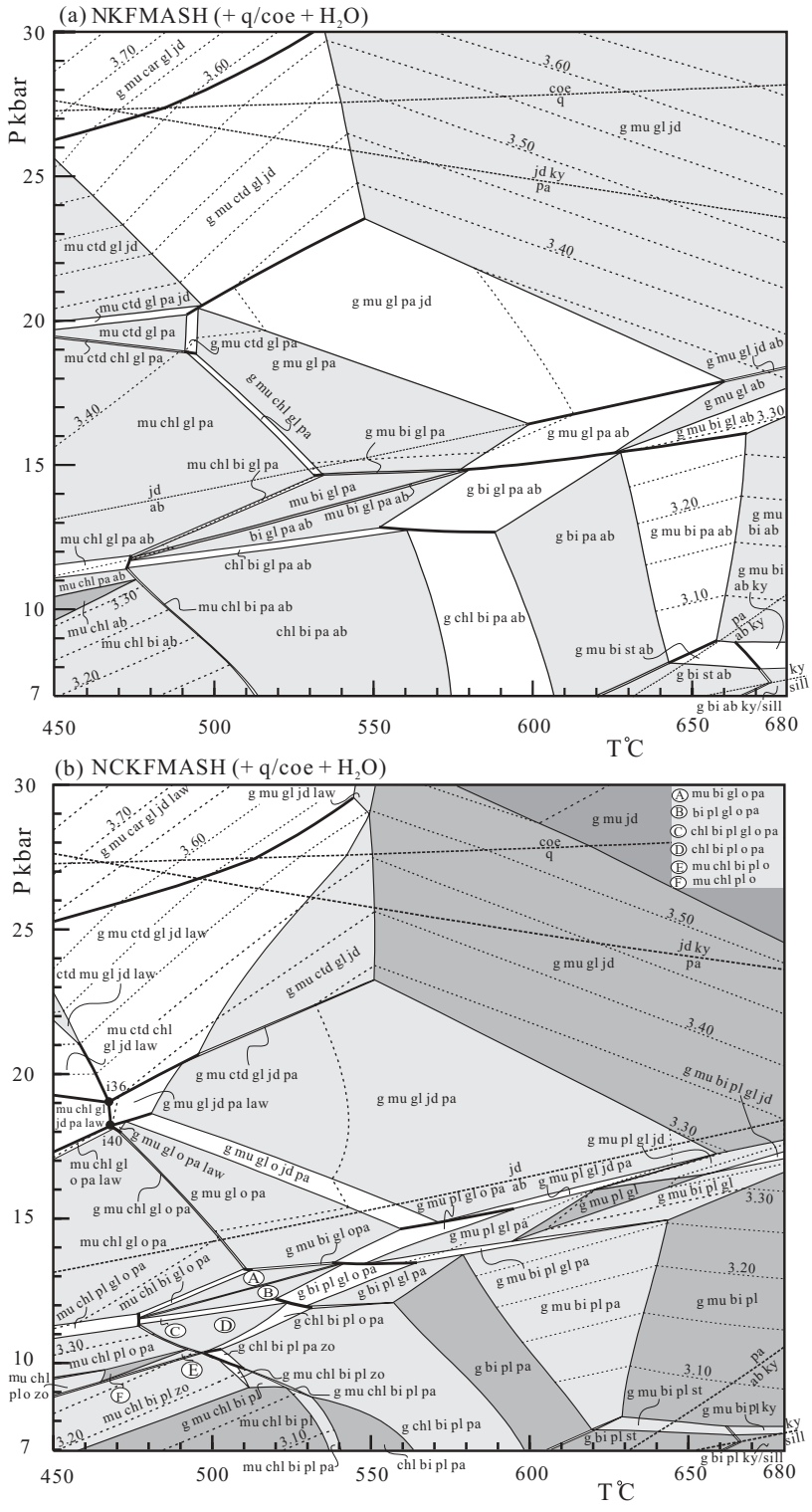

Fig. 6. NKFMASH (a) and NCKFMASH (b) *P–T* pseudosections for a glaucophane–phengite schist (sample AK07) from the Southern Tianshan, NW China, with Al_2O_3:MgO:FeO:K_2O:Na_2O = 34·79:14·88:30·58:4·58:15·16 in NKFMASH, and Al_2O_3:CaO:MgO:FeO:K_2O:Na_2O = 34·79:4·82:13·70:28·15:4·58:13·95 (mole basis) in NCKFMASH. The pseudosections show the invariant points (filled circles), univariant reactions (bold continuous lines), divariant fields (unshaded), trivariant fields (light grey shaded), quadrivariant fields (medium grey shaded) and quinivariant fields (dark grey shaded) encountered by the bulk composition. Isopleths of the Si content in phengitic muscovite are shown as the dashed lines with numbers such as (Si =) 3·40 p.f.u.

Downloaded from http://petrology.oxfordjournals.org/ at Indiana University School of Medicine Libraries on September 22, 2012

plagioclase when temperature is above 600°C. When temperature is below 600°C, jadeite is stable to lower pressure by 2–3 kbar, and transformed into omphacite through univariant reactions and/or a narrow divariant field g–mu–gl–o–jd–pa. Correspondingly, the stability fields of glaucophane and paragonite are reduced on the high-T side and plagioclase stability shrinks on the high-P side.

The effect of Ca on mineral stability is more clearly shown in T–X_{Ca} and P–X_{Ca} pseudosections (Fig. 7a and b) where $X_{Ca} = CaO/(CaO + Na_2O + FeO + MgO)$. In Fig. 7a, the low-$T$ limit of garnet is dependent on both X_{Ca} and mineral assemblage. It is at about 530°C in the Ca-free system, and dramatically decreases with X_{Ca} in the NCKFMASH trivariant assemblage g–mu–chl–pa–gl to about 495°C with $X_{Ca} \approx 0{\cdot}01$, when omphacite is stabilized. In the divariant assemblage g–mu–chl–o–pa–gl, the low-T limit of garnet is almost independent of X_{Ca}, then in the trivariant assemblage g–mu–chl–o–pa, the low-T limit of garnet decreases with X_{Ca} to about 480°C as $X_{Ca} \approx 0{\cdot}23$ to stabilize lawsonite, whereas in the lawsonite-bearing divariant assemblage g–mu–chl–o–pa–law, the low-T limit of garnet is independent of X_{Ca}. Similarly, jadeite and omphacite stabilities are strongly affected by X_{Ca}. As shown in Fig. 7a, jadeite is not present in the Ca-free system. However, it appears in a small field with $X_{Ca} \approx 0{\cdot}02$–$0{\cdot}15$ and $T \approx 540$–580°C. Omphacite becomes stable if even a small amount of CaO is added with $X_{Ca} \approx 0{\cdot}01$, and when $X_{Ca} > 0{\cdot}18$, omphacite will be stable in the entire temperature range of interest. In Fig. 7b, the low-P limit of jadeite in the Ca-free system controlled by the NAS reaction (jd + q = ab) is around 16·8 kbar, and in the Ca-bearing system, the low-P limit of jadeite decreases with X_{Ca} to ~0·22, and then mostly increases with X_{Ca} increasing. In addition, both Fig. 7a and Fig. 7b show that the stability fields of glaucophane, paragonite, plagioclase and the other AFM phases are reduced as X_{Ca} increases. For example, glaucophane will not be stable if $X_{Ca} > 0{\cdot}33$ in Fig. 7a and $X_{Ca} > 0{\cdot}30$ in Fig. 7b for the bulk-rock composition discussed.

The pseudosections are contoured for phengite Si isopleths. In Fig. 6a, the Si contents rise linearly with pressure in most tri- and divariant fields, but decrease with temperature in the divariant field g–mu–gl–pa–jd in the central part of Fig. 6a. The Si isopleths in Fig. 6b show a similar behavior to those in Fig. 6a. However, the NKFMASH phengite at the same P–T conditions is more Si-rich than the NCKFMASH phengite in the corresponding mineral assemblages. For example, at $P = 25$ kbar and $T = 610$°C, the NKFMASH phengite in the trivariant assemblage g–mu–gl–jd has Si = 3·48 in Fig. 6a, but the NCKFMASH phengite in the equivalent quadrivariant assemblage g–mu–gl–jd has Si = 3·45 in Fig. 6b, with the NKFMASH phengite decreasing its Si content at fixed P and T as CaO is incorporated.

The effect of Ca on the phengite Si content is clearly shown in Fig. 7b. For the assemblage g–mu–gl–jd, the phengite Si contents decrease slightly with X_{Ca} increasing at fixed P and T, for example, at 26 kbar and 610°C. This trend becomes much clearer in the assemblage g–mu–jd. In contrast, in the assemblage g–mu–jd–law, the phengite Si contents tend to increase with X_{Ca} but keep almost constant in the assemblage g–mu–o–jd–law. In the tri- and quadrivariant assemblages g–mu–gl–jd–pa, g–mu–o–jd–pa, g–mu–o–gl–pa, g–mu–o–pa and g–mu–o–pa–zo with pressures mostly between 15 and 20 kbar, the phengite Si isopleths decrease with X_{Ca} increasing and are almost independent of pressure. However, in the mineral assemblages g–mu–bi–pl–pa, g–mu–bi–pl and g–mu–bi–pl–zo with pressures mostly below 15 kbar, the phengite Si contents are constant or increase with X_{Ca} increasing, and rise linearly with pressure increasing. The phengite Si isopleths have shallow slopes, making the Si content a useful geobarometer. However, in the mineral assemblages at higher X_{Ca}, mostly those containing diopsidic clinopyroxene, the phengite Si isopleths vary inconsistently with X_{Ca} and pressure, depending on mineral assemblage. For example, the Si = 3·25 contour appears in fields at very different pressures, ranging from 7 to 23 kbar. As a consequence, the phengite Si contents could be used for geobarometry only if the strong dependence on mineral assemblage is taken into account.

The observed mineral assemblage g–mu–ab–gl for sample AK07 is trivariant in the NKFMASH system and makes up a small irregular triangle with P–T conditions above 16 kbar and >630°C in Fig. 6a, at a similar pressure but at a higher temperature than previous work (see above). In Fig. 6b, the observed assemblage is quadrivariant with P–T conditions of about 14·5–16·5 kbar and 600–650°C, which is in good agreement with the estimates of Wei *et al.* (2003). In Fig. 7a and b, the observed mineral assemblage is in a limited field involving a small X_{Ca} range from 0·03 to 0·12.

A metagranite from the Sesia–Lanzo Zone, Western Alps, Italy

The Sesia–Lanzo Zone in Italy represents the Adriatic continental margin of the Piemontese–Ligurian ocean, which is considered to have been subducted in the Late Cretaceous–Early Tertiary (Inger *et al.*, 1996; Duchêne *et al.*, 1997; Rubatto *et al.*, 1999). Related to the subduction event, a Permian intrusion of granitic to granodioritic composition exposed on Monte Mucrone was metamorphosed under high-pressure conditions. As described by Oberhänsli *et al.* (1985), the metagranitoids vary from rocks showing a well-preserved granitic texture

Downloaded from http://petrology.oxfordjournals.org/ at Indiana University School of Medicine Libraries on September 22, 2012

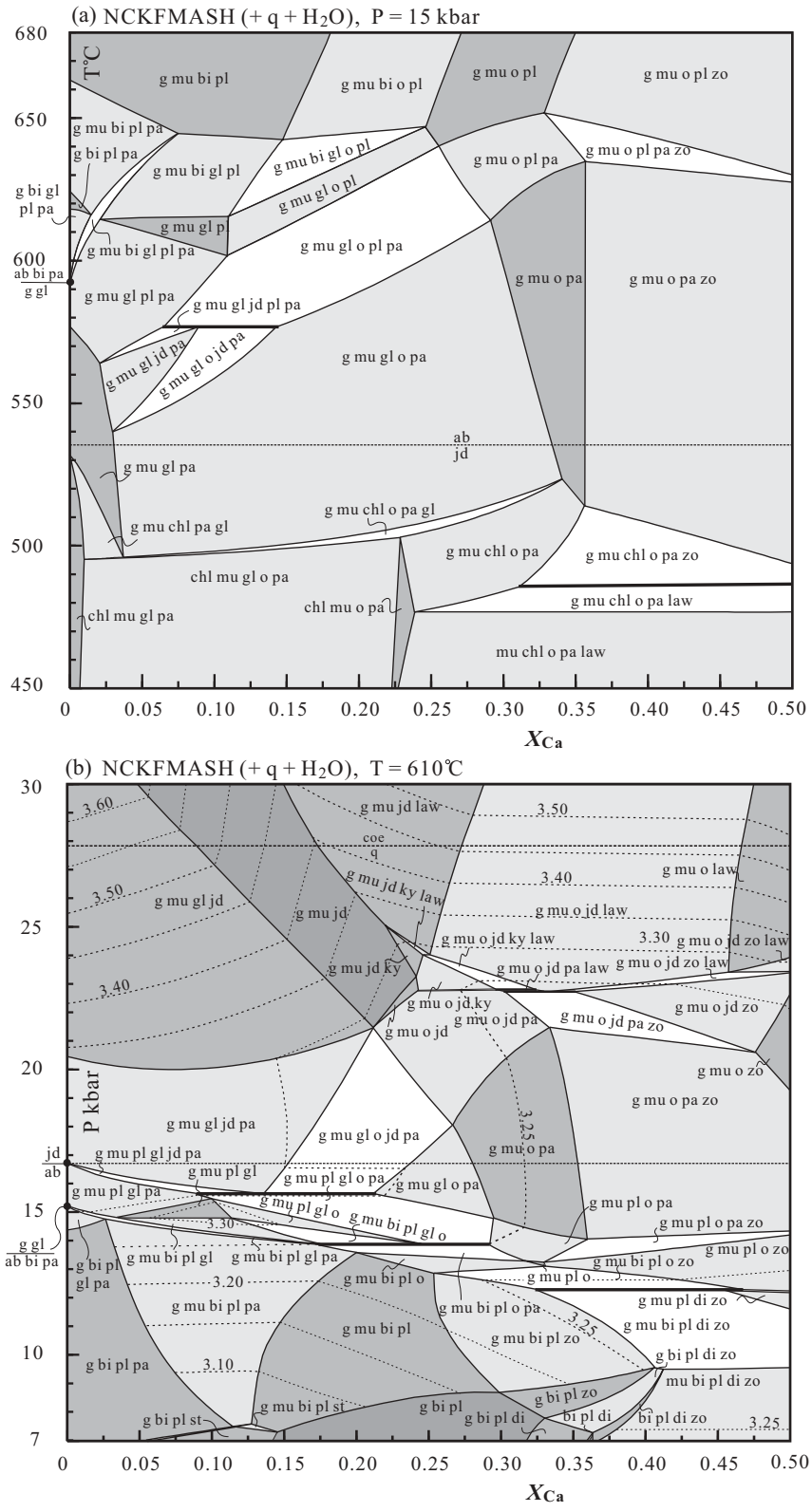

Fig. 7. T–X_{Ca} and P–X_{Ca} pseudosections in the NCKFMASH system calculated respectively at 15 kbar (a) and 610°C (b) for the glaucophane–phengite schist (sample AK07) with $X_{Ca} = [CaO/(MgO + FeO + CaO + Na_2O)]$ ranging from zero to 0·5. Small filled circles on the left border show the locations of univariant reactions in NKFMASH encountered by the bulk-rock composition. (For others see Fig. 6.)

Downloaded from http://petrology.oxfordjournals.org/ at Indiana University School of Medicine Libraries on September 22, 2012

to strongly deformed schists and gneisses. The least-transformed rocks that have a well-preserved granitic texture contain all the relict minerals of the original granite, e.g. biotite, K-feldspar, quartz, apatite, zircon, allanite and opaques, with the exception of plagioclase. This last mineral is pseudomorphed by aggregates of zoisite, jadeite and quartz. The completely recrystallized rocks contain the assemblage quartz + omphacite/jadeite + garnet + white mica + zoisite with some sphene and rutile. Oberhänsli *et al.* (1985) presented chemical analyses for 10 samples from the Mucrone rocks, all of which are similar. We selected a representative sample KAW988 with a bulk composition (in wt %) of SiO_2 68·3, Al_2O_3 15·2, Fe_2O_3 0·6, FeO 3·0, MgO 1·0, CaO 3·2, Na_2O 3·1 and K_2O 2·7, giving Al_2O_3:CaO:MgO:FeO:K_2O:Na_2O = 42·28:15·98:6·95:12·75:8·03:14·01 on a mole basis in NCKFMASH, in which the small amount of Fe_2O_3 is divided equally to Al_2O_3 and FeO. Using this bulk composition, a P–T pseudosection is calculated on the basis of the petrogenetic grid in Fig. 3a. For comparison, a P–T pseudosection of the NKFMASH grid (Wei & Powell, 2004) was calculated. To keep the internal consistency between P–T and $T(P)$–X_{Ca} pseudosections, the bulk composition in the Ca-free system was made in proportion, giving Al_2O_3:MgO:FeO:K_2O:Na_2O = 42·28:10·24:18·79:8·03:20·65. The two pseudosections are presented in Fig. 8a and b. The NKFMASH pseudosection in Fig. 8a is dominated by di- and trivariant fields with one quadrivariant field in the high P–T region. The P–T pseudosection in NCKFMASH (Fig. 8b) is dominated by di-, tri- and quadrivariant fields with one quinivariant field in the central part.

These two P–T pseudosections are significantly different from each other. In the Ca-free system (Fig. 8a), carpholite and chloritoid are stable in the high P–T part, and glaucophane and biotite are stable in much wider ranges than those in Fig. 8b, whereas in the Ca-bearing system, omphacite, diopsidic pyroxene, and zoisite/lawsonite are present. However, the stabilities of garnet, jadeite and paragonite are not simply enlarged as they were in the Tianshan sample AK07. As shown in Fig. 9a, the low-T limit of garnet is at about 530°C in the Ca-free system, and dramatically decreases with increasing X_{Ca} in the NCKFMASH trivariant assemblage g–gl–jd–pa to about 470°C. However, the garnet stability limit shows complicated relations with X_{Ca} when $X_{Ca} > \sim 0{\cdot}2$–$0{\cdot}3$ at temperatures below 600°C. Jadeite is stable in most fields in Fig. 9a except several fields in the center–right part with $X_{Ca} \approx 0{\cdot}30$–$0{\cdot}40$ and $T \approx 520$–610°C. Thus the effect of Ca on the stabilities of garnet and jadeite is dependent on mineral assemblage in some cases. Increasing X_{Ca} favors the stability of omphacite, and decreases the stability of glaucophane. When X_{Ca} is <0·12, glaucophane is stable in all of the temperature range in Fig. 9a; its stability fields reduce smoothly with increasing X_{Ca} and disappear when X_{Ca} is above 0·46. The high-T limit of paragonite in Fig. 9a increases with X_{Ca} in the assemblages lacking zoisite, g–gl–jd–pa and g–jd–pa, but decreases with X_{Ca} in the assemblages g–jd–pa–zo and g–o–jd–pa–zo where zoisite is present.

In the P–X_{Ca} pseudosection (Fig. 9b), the stabilities of garnet and jadeite are mostly enlarged with addition of Ca, but clearly this is dependent on mineral assemblage. For example, the low-P limit of jadeite is about 16·8 kbar controlled by the NAS reaction jd + q = ab in the NKFMASH system, decreases in the NCKFMASH assemblages g–pl–gl–jd–pa and g–pl–gl–jd, to about 15·7 kbar constrained by the univariant reaction i42(bi) jd + pa = g + pl + gl + o, but dramatically increases to about 19 kbar at X_{Ca} between 0·3 and 0·48, and then decreases to about 15·5 kbar. The high-P limit of glaucophane in the assemblages g–gl–jd, g–gl–jd–pa and g–gl–o–jd–pa decreases as X_{Ca} increases, but its low-P limit in the assemblages g–gl–bi–pl–pa, g–bi–pl–gl and g–bi–pl–gl–o changes trivially with X_{Ca} increasing. Glaucophane is not stable when X_{Ca} is above 0·25. Omphacite is stable only in a narrow pressure range between 14 and 16 kbar at a lower X_{Ca} of about 0·05–0·20, and its high-P limit enlarges with X_{Ca} above 0·20. Diopsidic clinopyroxene becomes stable at pressures lower than 12 kbar and X_{Ca} above 0·20. The stability of paragonite in Fig. 9b varies with mineral assemblage. For example, paragonite in the biotite-bearing assemblages bi–pl–pa, g–bi–pl–pa and g–gl–bi–pl–pa is stable at lower X_{Ca} (<0·06) and lower pressures below 15·2 kbar, and paragonite in the biotite-absent assemblages at pressures between 14 and 23 kbar expands its stability with X_{Ca} increasing in the assemblages such as g–gl–jd–pa and g–jd–pa that lack zoisite or lawsonite. However, the stability of paragonite shrinks significantly with X_{Ca} in assemblages with these Ca-phases such as g–o–jd–pa–zo and g–pl–o–pa–zo.

These pseudosections are contoured for the phengite Si isopleths. In Fig. 8a, the Si contents rise linearly with pressure in the paragonite-out assemblages in the high-pressure part and in the biotite/albite-bearing assemblages in the lower-pressure fields, but decrease with temperature in the assemblages g–mu–gl–pa–jd and g–gl–ab. The Si isopleths in phengite in Fig. 8b rise linearly with pressure only in the lawsonite-bearing high-pressure assemblages, but change in an inconsistent way in the assemblages at lower pressures, especially in the diopsidic pyroxene-bearing assemblages where the Si isopleths in phengite even decrease with pressure. In Fig. 9b, there only a few mineral assemblages where the phengite Si isopleths could be used geobarometrically, and they vary inconsistently in the other assemblages with pressure.

A comparison of the two NKFMASH P–T pseudosections in Figs 6a and 8a, and of the two P–X_{Ca} pseudosections in Figs 7b and 9b, shows that the phengite Si

Downloaded from http://petrology.oxfordjournals.org/ at Indiana University School of Medicine Libraries on September 22, 2012

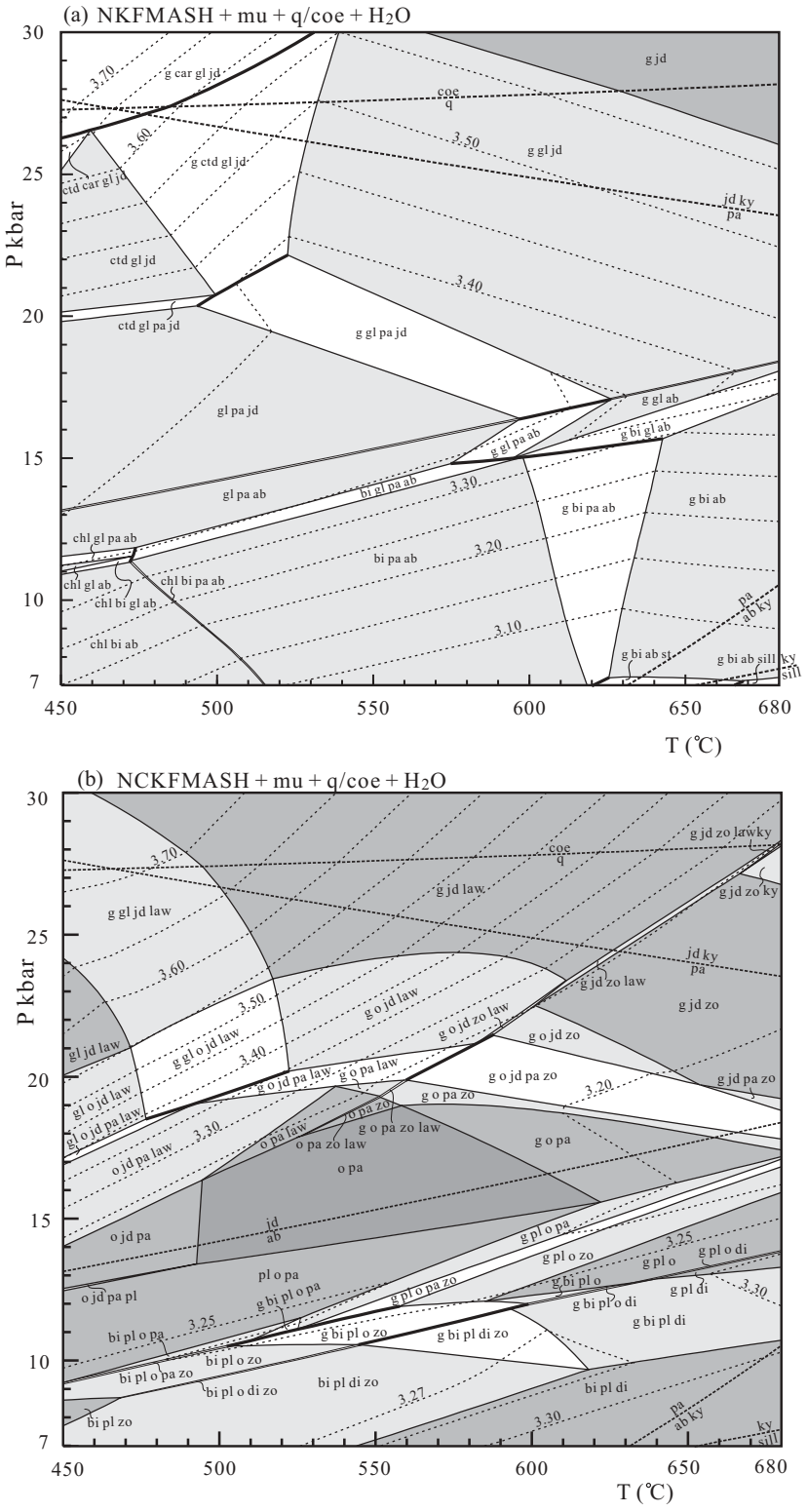

Fig. 8. NKFMASH (a) and NCKFMASH (b) *P–T* pseudosections for a metagranite (sample KAW988) from the Sesia–Lanzo Zone, Western Alps, Italy (Oberhänsli *et al.*, 1985) with Al_2O_3:MgO:FeO:K_2O:Na_2O = 42·28:10·24:18·79:8·03:20·65 in NKFMASH, and Al_2O_3:CaO:MgO:FeO:K_2O:Na_2O = 42·28:15·98:6·95:12·75:8·03:14·01 (mole basis) in NCKFMASH. The pseudosections show the univariant reactions (bold continuous lines), divariant fields (unshaded), trivariant fields (light grey shaded), quadrivariant fields (medium grey shaded) and quinivariant fields (dark grey shaded) encountered by the bulk composition. Isopleths of the Si content in phengitic muscovite are shown as the dashed lines with numbers such as (Si =) 3·40 p.f.u.

Downloaded from http://petrology.oxfordjournals.org/ at Indiana University School of Medicine Libraries on September 22, 2012

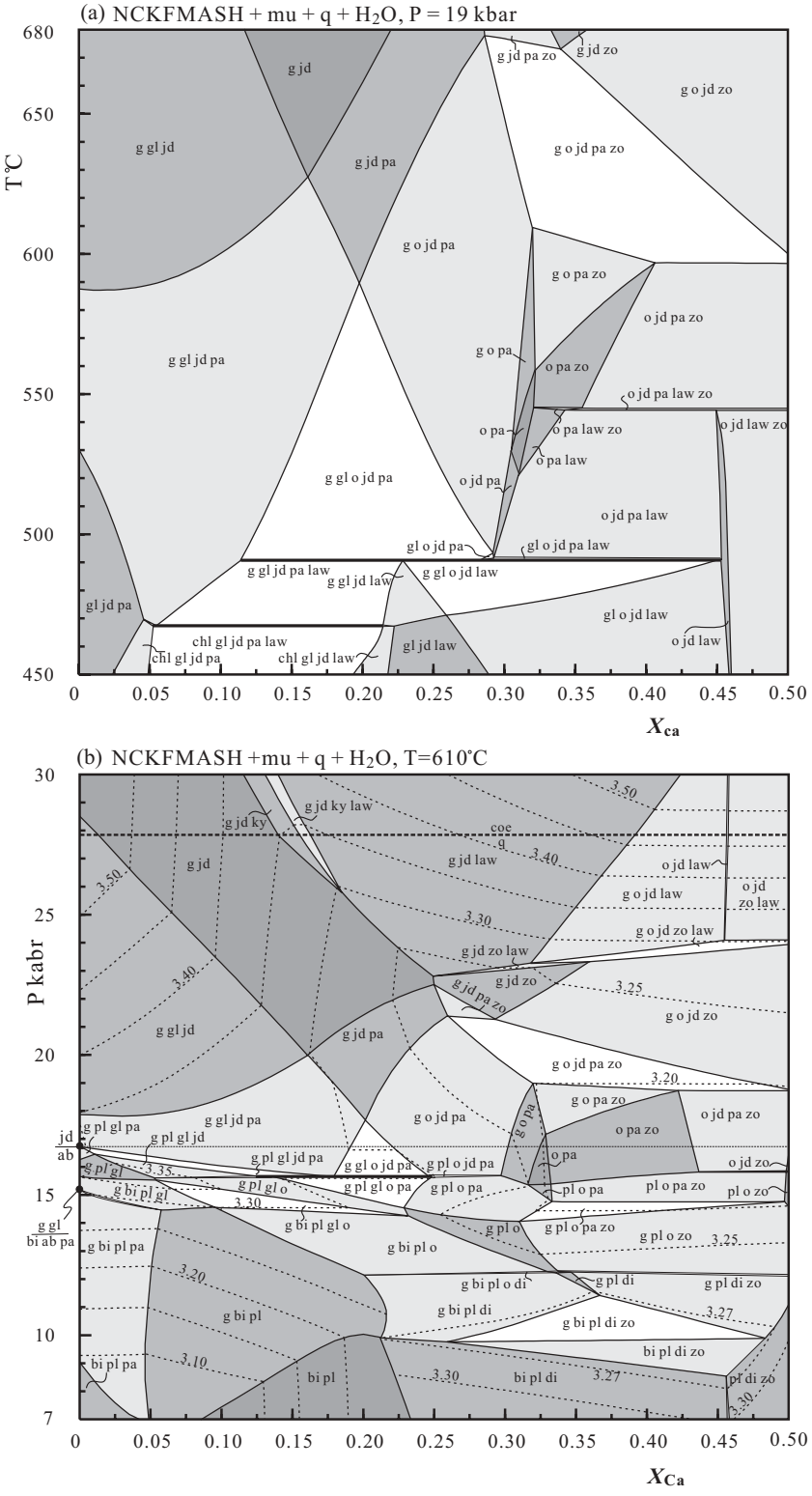

Fig. 9. T–X_{Ca} and P–X_{Ca} pseudosections in the NCKFMASH system calculated respectively at 19 kbar (a) and 610°C (b) for the metagranite (sample KAW988) from the Sesia–Lanzo Zone, Western Alps, with X_{Ca} = [CaO/(MgO + FeO + CaO + Na_2O)] ranging from zero to 0·5. Small filled circles on the left border show the locations of univariant reactions in NKFMASH encountered by the bulk-rock composition. (For the others see Fig. 8.)

Downloaded from http://petrology.oxfordjournals.org/ at Indiana University School of Medicine Libraries on September 22, 2012

isopleths in the same mineral assemblages indicate different pressures at the same temperature. For example, the isopleth of Si = 3·40 in the trivariant assemblage g–mu–gl–jd in Fig. 7a provides a pressure of 22·5 kbar at T = 610°C, whereas the same Si isopleth in the same assemblage in Fig. 9a gives a pressure of 20 kbar at T = 610°C. This is related to the dependence of the Si value on bulk-rock composition if the phengite composition is not buffered by the assemblage (if its variance is greater than two).

The observed mineral assemblage garnet + Na-pyroxene (from jadeite to omphacite) + white mica (phengite/paragonite) + zoisite in the Monte Mucrone metagranite approximates to the tri- and divariant fields g–o–pa–zo, g–o–jd–pa–zo and g–o–jd–zo (+ phengite + quartz), with temperatures above 550°C and pressures in the range of 17–22 kbar. At T = 600°C, jadeite disappears at pressures below 19 kbar and paragonite disappears at pressures above 21 kbar. These values are in agreement with the estimates of 600–620°C and 17·5–18·5 kbar for such quartzofeldspathic rocks by Koons (1986) in a neighboring area. The pressure of ~14 kbar at 600°C for the peak of the eclogite metamorphism of Oberhänsli *et al.* (1985) was probably underestimated. In Fig. 9a and b, the observed mineral assemblages could be present in zoisite-bearing rocks with $X_{Ca} > 0{\cdot}25$–$0{\cdot}30$. For $X_{Ca} < 0{\cdot}2$, the predicted mineral assemblage at the same P–T conditions is g + gl + jd + pa + mu + q, which is that described by Koons (1986) in quartzofeldspathic rocks from the Sesia–Lanzo Zone.

DISCUSSION AND CONCLUSION

Comparison with published petrogenetic grids

Will *et al.* (1998) presented an NCFMASH grid for the P–T range 4–23 kbar and 380–620°C using THERMOCALC and the thermodynamic dataset of Holland & Powell (1990). In their grid, all the six comparable invariant equilibria, including two CFMASH (+ q + H_2O) equilibria (g–chl–ta–zo–ky–law and g–chl–ctd–zo–ky–law) and four NCFMASH (+ q + H_2O) equilibria (g–gl–ctd–chl–pa–ky–law, g–gl–chl–pa–ky–zo–law, ctd–gl–chl–pa–car–o–law and ctd–gl–chl–pa–car–ky–law), are metastable in the present study. As a consequence, the grid in Fig. 3a is considerably different from that presented by Will *et al.* (1998). The principal dissimilarity between the two grids comes from reaction chl + ky = ctd + ta that connects invariant points i2 and i5 in Fig. 3a. As already determined by Guiraud *et al.* (1990) using the database of Holland & Powell (1990), this reaction was found to occur at much higher pressures (up to 28 kbar). This results in the phase topologies, especially the part shown in Fig. 3a, being significantly different. The new grids, involving a better dataset and activity–composition relationships for the minerals, in this case particularly for chlorite, provide a substantial improvement. In addition, as has been noted by Wei & Powell (2004), the involvement of K_2O and the relevant phases phengite and biotite in our study provides more constraints on the lower-P part of the grid, for instance, the equilibria mostly below the reaction jd + q = ab.

High-P assemblages in Ca-bearing metapelites

As documented above, incorporation of Ca into the NKFMASH system with the relevant Ca-bearing phases omphacite, diopsidic pyroxene, lawsonite and zoisite leads to much more complicated phase relations in the NCKFMASH system. Many NKFMASH invariant equilibria move to lower pressures and/or lower temperatures, which, in most cases, results in the enlargement of stability of jadeite and garnet, but in the reduction of stability of glaucophane, plagioclase and AFM phases. The effect of Ca on the stability of paragonite is complex. Paragonite in the plagioclase- and biotite-bearing assemblages at lower pressures (<15 kbar) is favored by lower CaO content. In the jadeite- and/or omphacite-bearing assemblages at higher pressures mostly between 14–22 kbar, the stability of paragonite expands as X_{Ca} rises until zoisite or lawsonite are involved, then it contracts with increasing X_{Ca}. As shown in Figs 7a and b and 9a and b, the effect of Ca on phase relations is dependent on Ca content and mineral assemblage. For jadeite and garnet, the Ca effect is even more obvious when X_{Ca} is very small. As CaO has to be already relatively high to stabilize zoisite or lawsonite, the mineral stabilities are less affected by X_{Ca}, but these assemblages are usually not matched with the Ca-free ones. As a consequence, even a rock that contains a small amount of CaO, such as AK07, will be better delineated in NCKFMASH than in NKFMASH. A rock with a higher CaO content, such as KAW988, can only be accounted for in the Ca-bearing system.

The present NCKFMASH grid can be applied to other mineral assemblages reported from natural Na-rich metapelites; some of these that have been highlighted by Proyer (2003) and Wei & Powell (2004) are briefly reconsidered below.

Chloritoid + jadeite

Okay (2002) described a particular sodic metapelite from NW Turkey with a mineral assemblage of jd [0·85 < j(o) < 0·98] + ctd + gl + chl + mu + law + q (samples 4892B and 4893B). If the only Ca-rich phase, lawsonite, is ignored, the other six NKFMASH phases constitute a divariant assemblage with P–T in the range of 19–26 kbar and 410–480°C (see Wei & Powell, 2004, fig. 3). In the NCKFMASH system, the assemblage is also divariant with its high-T and low-P limits constrained by reactions

Downloaded from http://petrology.oxfordjournals.org/ at Indiana University School of Medicine Libraries on September 22, 2012

i36(pa) chl + jd + law = g + ctd + gl and i36(g) ctd + gl + jd = chl + pa + law, below 470°C and above 19 kbar, slightly lower than the P–T condition in the NKFMASH. The calculated jadeite has j(jd) > 0·9 (see i36 in Table 3), in agreement with the measured value in the assemblage.

Chloritoid + glaucophane

This assemblage is one of the most common high-pressure indicators in metapelites and has been reported in various parts of the world (Wei & Powell, 2004). The low-P limit for this paragenesis is about 18–19 kbar according to the thermodynamic calculations in N(K)FMASH (Guiraud *et al.*, 1990; Proyer, 2003; Wei & Powell, 2004). As constrained by reactions i36(g) ctd + gl + jd = chl + pa + law, i15(zo) ctd + gl + law = g + chl + pa, i15(law) ctd + gl + zo = g + chl + pa and i14(zo) ctd + gl + ky = g + chl + pa in NCKFMASH (Fig. 3b), the low-P limit for chloritoid + glaucophane is similar to that in NKFMASH, but the temperature divisions are clearer. With temperature increase, chloritoid + glaucophane will coexist successively with jadeite, lawsonite and zoisite as well as kyanite. Most natural occurrences of chloritoid + glaucophane coexist with zoisite or epidote (Kiénast & Triboulet, 1972; El-Shazly & Liou, 1991), suggesting a narrow P–T range of 550–600°C and 18–22 kbar limited by the univariant reactions connecting invariant points i15, i23, i22, i2 and i14 in Fig. 3b. As all of the three phases chloritoid, glaucophane and epidote can incorporate significant amounts of Fe^{3+}, this field expands considerably to lower pressures with rising X^{3+}_{Fe}, as discussed qualitatively by Guiraud *et al.* (1990).

Jadeite + kyanite and omphacite + kyanite

As mentioned above, the stability of the assemblage jadeite + kyanite is extended in the Ca-bearing system, as a consequence of a series of reactions involving paragonite with combinations of carpholite, chloritoid, lawsonite, glaucophane, garnet, zoisite and omphacite in Fig. 3a [i37(gl), i35(g), i38(o) and i38(law)]. The assemblage omphacite + kyanite or kyanite eclogite is bounded by reactions i38(pa) g + gl + jd + law = o + ky, i21(zo) g + gl + pa + law = o + ky and i21(law) g + gl + pa + zo = o + ky, with P–T condition above 18 kbar and 590°C, which is analogous to that calculated by Wei *et al.* (2003) and also consistent with the estimated P–T conditions of >600°C, >20 kbar and high $a(H_2O)$ for kyanite-bearing eclogite from natural occurrences and experimental studies (Holland, 1979, 1988).

Phengite geobarometry in the NCKFMASH system

The experimental calibrations of the phengite Si contents in limited KMASH assemblages (Massonne & Schreyer, 1987, 1989; Massonne & Szpurzka, 1997) show that phengite has a potential for geobarometry. This was supported by the calculated results in the KMASH and KFMASH systems (Wei & Powell, 2003). According to the calculations in the NKFMASH system, however, Wei & Powell (2004) showed that phengite geobarometry is highly dependent on mineral assemblage. The present study confirms this conclusion. The phengite Si contours in the P–T and P–X_{Ca} pseudosections for the two selected samples indicate that phengite barometry seems to have potential only in the higher-pressure paragonite-absent mineral assemblages and lower-pressure biotite- and plagioclase-bearing, lower-X_{Ca} assemblages, as shown in Figs 6a and b, 7b, 8a and 9b, or higher-pressure lawsonite-stable assemblages as shown in Fig. 8b. Indiscriminate use of the Si-in-phengite barometer is ill-advised.

ACKNOWLEDGEMENTS

This work was financially supported by the National Natural Science Foundation of China (40372132) and by the 'Major State Basic Research Development Program of China' (G1999075508). We are grateful to Chris Carson and Frank Spear for constructive reviews of the manuscript. Dr Geoffrey Clarke is thanked for his careful editorial work.

REFERENCES

Abraham, K. & Schreyer, W. (1976). A talc–phengite assemblage in piemontite schist from Brezovica, Serbia, Yugoslavia. *Journal of Petrology* **17**, 421–439.

Carson, C. J., Powell, R. & Clarke, G. L. (1999). Calculated mineral equilibria for eclogites in CaO–Na_2O–FeO–MgO–Al_2O_3–SiO_2–H_2O: application to the Pouébo Terrane, Pam Peninsula, New Caledonia. *Journal of Metamorphic Geology* **17**, 9–24.

Chopin, C. (1981). Talc–phengite: a widespread assemblage in high-grade pelitic blueschists of the western Alps. *Journal of Petrology* **22**, 628–650.

Chopin, C. (1984). Coesite and pure pyrope in high-grade blueschists of the Western Alps: a first record and some consequences. *Contributions to Mineralogy and Petrology* **86**, 107–118.

Chopin, C. & Schreyer, W. (1983). Magnesiocarpholite and magnesiochloritoid: two index minerals of pelitic blueschists and their preliminary phase relations in the model system MgO–Al_2O_3–SiO_2–H_2O. *American Journal of Science* **283-A**(Orville volume), 72–96.

Coggon, R. & Holland, T. J. B. (2002). Mixing properties of phengitic micas and revised garnet–phengite thermobarometers. *Journal of Metamorphic Geology* **20**, 683–696.

Compagnoni, R. & Rolfo, F. (2000). Characteristics of UHP pelites, gneisses and other unusual rocks. In: Ernst, G. & Liou, J. G. (eds) *Ultra-High Pressure Metamorphism and Geodynamics in Collision-Type Orogenic Belts*. Columbia, MD: Bellwether, pp. 74–94.

Dale, J., Holland, T. & Powell, R. (2000). Hornblende–garnet–plagioclase-thermobarometry: a natural assemblage calibration of the thermodynamics of hornblende. *Contributions to Mineralogy and Petrology* **140**, 353–362.

Duchêne, S., Blichert-Toft, J., Luais, B., Télouk, P., Lardeaux, J.-M. & Albarède, F. (1997). The Lu–Hf dating of garnets and the ages of the Alpine high-pressure metamorphism. *Nature* **387**, 586–589.

Downloaded from http://petrology.oxfordjournals.org/ at Indiana University School of Medicine Libraries on September 22, 2012

El-Shazly, A. K. & Liou, J. G. (1991). Glaucophane chloritoid-bearing assemblages from NE Oman: petrologic significance and a petrogenetic grid for high-*P* metapelites. *Contributions to Mineralogy and Petrology* **107**, 180–201.

Gao, J., He, G., Li, M., Xiao, X., Tang, Y., Zhou, M. & Wang, J. (1995). The mineralogy, petrology, metamorphic *PTDt* trajectory and exhumation mechanism of blueschists, south Tianshan, northwestern China. *Tectonophysics* **250**, 151–168.

Gao, J., Klemd, R., Zhang, L., Wang, Z. & Xiao, X. (1999). *P–T* path of high-pressure/low-temperature rocks and tectonic implications in the western Tianshan Mountains, NW China. *Journal of Metamorphic Geology* **17**, 621–636.

Guiraud, M., Holland, T. J. B. & Powell, R. (1990). Calculated mineral equilibria in the greenschist–blueschist–eclogite facies in Na_2O–FeO–MgO–Al_2O_3–SiO_2–H_2O: methods, results and geological applications. *Contributions to Mineralogy and Petrology* **104**, 85–98.

Hermann, J. (2002). Experimental constraints on phase relations in subducted continental crust. *Contributions to Mineralogy and Petrology* **143**, 219–235.

Holland, T. J. B. (1979). Experimental determination of the reaction paragonite = jadeite + kyanite + quartz + water, and internally consistent thermodynamic data for part of the system Na_2O–Al_2O_3–SiO_2–H_2O, with applications to eclogites and blueschists. *Contributions to Mineralogy and Petrology* **68**, 293–301.

Holland, T. J. B. (1988). Preliminary phase relations involving glaucophane and applications to high pressure petrology: new heat capacity and thermodynamic data. *Contributions to Mineralogy and Petrology* **99**, 134–142.

Holland, T. J. B. & Powell, R. (1990). An enlarged and updated internally consistent thermodynamic dataset with uncertainties and correlations: the system K_2O–Na_2O–CaO–MgO–MnO–FeO–Fe_2O_3–Al_2O_3–TiO_2–SiO_2–C–H_2–O_2. *Journal of Metamorphic Geology* **8**, 89–124.

Holland, T. J. B. & Powell, R. (1992). Plagioclase feldspar: activity–composition relations based upon Darken's quadratic formalism and Landau theory. *American Mineralogist* **77**, 53–61.

Holland, T. J. B. & Powell, R. (1996). Thermodynamics of order–disorder in minerals: II. Symmetric formalism applied to solid solutions. *American Mineralogist* **81**, 1425–1437.

Holland, T. J. B. & Powell, R. (1998). An internally consistent thermodynamic data set for phases of petrological interest. *Journal of Metamorphic Geology* **16**, 309–343.

Holland, T. J. B., Barker, J. & Powell, R. (1998). Mixing properties and activity–composition relationships of chlorites in the system MgO–FeO–Al_2O_3–SiO_2–H_2O. *European Journal of Mineralogy* **10**, 395–406.

Inger, S., Ramsbotham, W., Cliff, R. A. & Rex, D. C. (1996). Metamorphic evolution of the Sesia–Lanzo Zone, Western Alps: time constraints from multi-system geochronology. *Contributions to Mineralogy and Petrology* **126**, 152–168.

Kiénast, J. R. & Triboulet, C. (1972). Le chloritoïde dans les paragenèses à glaucophane, albite ou paragonite. *Bulletin de la Société Française de Minéralogie et de Cristallographie* **95**, 565–573.

Klemd, R., Schröter, F. C., Will, T. M. & Gao, J. (2002). *P–T* evolution of glaucophane–omphacite bearing *HP–LT* rocks in the western Tianshan Orogen, NW China: new evidence for 'Alpine-type' tectonics. *Journal of Metamorphic Geology* **20**, 239–254.

Koons, P. O. (1986). Relative geobarometry from high-pressure rocks of quartzofeldspathic composition from the Sesia–Lanzo Zone, Western Alps, Italy. *Contributions to Mineralogy and Petrology* **93**, 322–334.

Kulke, H. & Schreyer, W. (1973). Kyanite–talc–schist from Sar E Sang, Afghanistan. *Earth and Planetary Science Letters* **18**, 324–328.

Liu, F. L., Xu, Z. Q., Katayama, I., Yang, J. S., Maruyama, S. & Liou, J. G. (2001). Mineral inclusions in zircons of para- and orthogneiss from pre-pilot drillhole CCSD-PP1, Chinese Continental Scientific Drilling Project. *Lithos* **59**, 199–215.

Mahar, E. M., Baker, J. M., Powell, R., Holland, T. J. B. & Howell, N. (1997). The effect of Mn on mineral stability in metapelites. *Journal of Metamorphic Geology* **15**, 223–238.

Massonne, H. J. (1995). Experimental and petrologic study of UHPM. In: Coleman, R. & Wang, X. (eds) Ultrahigh Pressure Metamorphism. Cambridge: Cambridge University Press, pp. 33–95.

Massonne, H. J. (2000). Experimental aspects of UHP metamorphism in pelitic systems. In: Ernst, W. G. & Liou, J. G. (eds) *Ultrahigh-pressure Metamorphism and Geodynamics in Collision-type Orogenic Belts*. Columbia, MD: Bellwether, pp. 105–120.

Massonne, H. J. & Schreyer, W. (1987). Phengite geobarometry based on the limiting assemblages with K-feldspar, phlogopite and quartz. *Contributions to Mineralogy and Petrology* **96**, 212–224.

Massonne, H. J. & Schreyer, W. (1989). Stability field of the high-pressure assemblage talc–phengite and two new phengite barometers. *European Journal of Mineralogy* **1**, 391–410.

Massonne, H. J. & Szpurzka, Z. (1997). Thermodynamic properties of white micas on the basis of high-pressure experiments in the systems K_2O–MgO–Al_2O_3–SiO_2–H_2O and K_2O–FeO–Al_2O_3–SiO_2–H_2O. *Lithos* **41**, 229–250.

Oberhänsli, R., Hunziker, J. C., Martinotti, G. & Stern, W. B. (1985). Geochemistry, geochronology, and petrology of Monte Mucrone: an example of Eo-Alpine eclogitization of Permian granitoids in the Sesia–Lanzo zone, Western Alps, Italy. *Chemical Geology* **52**, 165–184.

Okay, A. I. (2002). Jadeite–chloritoid–glaucophane–lawsonite blueschists in northwestern Turkey: unusually high *P/T* ratios in continental crust. *Journal of Metamorphic Geology* **20**, 757–768.

Powell, R. (1987). Darken's quadratic formalism and the thermodynamics of minerals. *American Mineralogist* **72**, 1–11.

Powell, R. & Holland, T. J. B. (1990). Calculated mineral equilibria in the pelitic system KFMASH (K_2O–FeO–MgO–Al_2O_3–SiO_2–H_2O). *American Mineralogist* **75**, 367–380.

Powell, R. & Holland, T. J. B. (1999). Relating formulations of the thermodynamics of mineral solid solutions: activity modeling of pyroxenes, amphiboles, and micas. *American Mineralogist* **84**, 1–14.

Powell, R., Holland, T. & Worley, B. (1998). Calculating phase diagram involving solid solutions via non-linear equations, with examples using THERMOCALC. *Journal of Metamorphic Geology* **16**, 577–586.

Proyer, A. (2003). Metamorphism of pelites in NKFMASH—a new petrogenetic grid with implications for the preservation of high-pressure mineral assemblages during exhumation. *Journal of Metamorphic Geology* **21**, 493–509.

Rubatto, D., Gebauer, D. & Compagnoni, R. (1999). Dating of eclogite-facies zircons: the age of Alpine metamorphism in the Sesia–Lanzo Zone (Western Alps). *Earth and Planetary Science Letters* **167**, 141–158.

Schreyer, W. (1977). Whiteschists: their compositions and pressure–temperature regimes based on experimental, field and petrographic evidence. *Tectonophysics* **34**, 127–144.

Schreyer, W. (1988). Experimental studies on metamorphism of crustal rocks under mantle pressures. *Mineralogical Magazine* **52**, 1–26.

Vance, D. & Holland, T. J B. (1993). A detailed isotopic and petrological study of a single garnet from the Gassetts Schist, Vermont. *Contributions to Mineralogy and Petrology* **114**, 101–118.

Wei, C. J. & Powell, R. (2003). Phase relations in high-pressure metapelites in the system KFMASH (K_2O–FeO–MgO–Al_2O_3–SiO_2–H_2O) with application to natural rocks. *Contributions to Mineralogy and Petrology* **145**, 301–315.

Wei, C. J. & Powell, R. (2004). Calculated phase relations in high-pressure metapelites in the system NKFMASH

Downloaded from http://petrology.oxfordjournals.org/ at Indiana University School of Medicine Libraries on September 22, 2012

(Na_2O–K_2O–FeO–MgO–Al_2O_3–SiO_2–H_2O) with application to natural rocks. *Journal of Petrology* **44**, 183–202.

Wei, C. J., Powell, R. & Zhang, L. F. (2003). Eclogites from the south Tianshan, NW China: petrological characteristic and calculated mineral equilibria in the Na_2O–CaO–FeO–MgO–Al_2O_3–SiO_2–H_2O system. *Journal of Metamorphic Geology* **21**, 163–180.

White, R. W., Powell, R. & Holland, T. J. B. (2001). Calculation of partial melting equilibria in the system Na_2O–CaO–K_2O–FeO–MgO–Al_2O_3–SiO_2–H_2O (NCKFMASH). *Journal of Metamorphic Geology* **19**, 139–153.

Will, T., Okrusch, M., Schmädicke, E. & Chen, G. (1998). Phase relations in the greenschist–blueschist–amphibolite–eclogite facies in the system Na_2O–CaO–FeO–MgO–Al_2O_3–SiO_2–H_2O (NCFMASH), with application to metamorphic rocks from Samos, Greece. *Contributions to Mineralogy and Petrology* **132**, 85–102.

Xu, G., Will, T. M. & Powell, R. (1994). A calculated petrogenetic grid for the system K_2O–FeO–MgO–Al_2O_3–SiO_2–H_2O, with particular reference to contact-metamorphosed pelites. *Journal of Metamorphic Geology* **12**, 99–119.

Zhang, L. F., Ellis, D. J. & Jiang, W. B. (2002*a*). Ultrahigh-pressure metamorphism in western Tianshan, China, Part I: evidence from inclusions of coesite pseudomorphs in garnet and from quartz exsolution lamellae in omphacite in eclogites. *American Mineralogist* **87**, 853–860.

Zhang, L. F., Ellis, D. J., Williams, S. & Jiang, W. B. (2002*b*). Ultrahigh-pressure metamorphism in western Tianshan, China, Part II: evidence from magnesite in eclogite. *American Mineralogist* **87**, 861–866.

APPENDIX: MIXING MODELS, AND MINERAL AND END-MEMBER FORMULAE

Garnet (*g*): $[Mg,Fe,Ca]_3Al_2Si_3O_{12}$

A symmetric solution model is used for Mg–Fe–Ca mixing in ternary garnet in which Ca–Mg and Fe–Mg interactions are taken to be non-ideal with the interaction parameters W(py, gr) = 33 kJ/mol and W(py, alm) = 2·5 kJ/mol following Dale *et al.* (2000). The end-members are:

pyrope (py): $Mg_3Al_2Si_3O_{12}$;
almandine (alm): $Fe_3Al_2Si_3O_{12}$;
grossular (gr): $Ca_3Al_2Si_3O_{12}$.

Compositional variables are x(g) = Fe/(Mg + Fe + Ca) and z(g) = Ca/(Mg + Fe + Ca).

Chloritoid (ctd): $[Fe,Mg]Al_2SiO_5(OH)_2$

A symmetric solution model is used for Mg–Fe mixing in binary chloritoid with the interaction parameter W(mctd, fctd) = 1·0 kJ/mol following Holland & Powell (1998). End-members are:

Mg-chloritoid (mctd): $MgAl_2SiO_5(OH)_2$;
Fe-chloritoid (fctd): $FeAl_2SiO_5(OH)_2$.

Composition variable is x(ctd) = Fe/(Mg + Fe).

Carpholite (car): $[Fe,Mg]Al_2Si_2O_6(OH)_4$

Mg–Fe mixing in carpholite is assumed to be ideal. End-members are:

Mg-carpholite (mcar): $MgAl_2Si_2O_6(OH)_4$;
Fe-carpholite (fcar): $FeAl_2Si_2O_6(OH)_4$.

Composition variable is x(car) = Fe/(Mg + Fe).

Chlorite (chl): $[Fe,Mg,]_4^{M2,3}[Mg,Fe,Al]_2^{M1,4}[Si,Al]_2^{T1}Si_2^{T2}O_{10}(OH)_8$

According to Holland *et al.* (1998), the thermodynamics of ordered chlorite are modeled using a quaternary symmetric mixing model. End-members are:

Al-free chlorite (afchl): $[Mg]_4^{M2,3}[Mg]^{M1}[Mg]^{M4}[Si]_2^{T1}[Si]_2^{T2}O_{10}(OH)_8$;
clinochlore (clin): $[Mg]_4^{M2,3}[Mg]^{M1}[Al]^{M4}[Al]^{T1}[Si]^{T1}[Si]_2^{T2}O_{10}(OH)_8$;
daphnite (daph): $[Fe]_4^{M2,3}[Fe]^{M1}[Al]^{M4}[Al]^{T1}[Si]^{T1}[Si]_2^{T2}O_{10}(OH)_8$;
amesite (ames): $[Mg]_4^{M2,3}[Al]^{M1}[Al]^{M4}[Al]_2^{T1}[Si]_2^{T2}O_{10}(OH)_8$.

Interaction parameters: W(afchl, clin) = 18 kJ/mol, W(afchl, daph) = 14·5 kJ/mol, W(afchl, ames) = 20 kJ/mol, W(clin, daph) = 2·5 kJ/mol, W(clin, ames) = 18 kJ/mol and W(daph, ames) = 13·5 kJ/mol. Composition variables: x(chl) = Fe/(Fe + Mg), y(chl) = x_{Al}^{T2} = Al/4 and N(chl) = $(x_{Al}^{M4} - x_{Al}^{M1})/2$.

Talc (ta): $[Fe,Mg]_2^{M1}[Fe,Mg,Al]^{M3}[Si,Al]_2^{T1}[Si]_2^{T2}O_{10}(OH)_2$

Following Holland & Powell (1998), an ideal mixing model is used for the ternary talc in which the Al is assumed to order onto the M3 site and to enter only the two T1 sites. End-members are:

talc (ta): $[Mg]_2^{M1}[Mg]^{M3}[Si]_2^{T1}[Si]_2^{T2}O_{10}(OH)_2$;
Fe-talc (fta): $[Fe]_2^{M1}[Fe]^{M3}[Si]_2^{T1}[Si]_2^{T2}O_{10}(OH)_2$;
Tschermak-talc (tats): $[Mg]_2^{M1}[Al]^{M3}[Al]^{T1}[Si]^{T1}[Si]_2^{T2}O_{10}(OH)_2$.

Composition variables are x(ta) = Fe/(Fe + Mg) and y(ta) = x_{Al}^{M3}.

Staurolite (st): $[Fe,Mg]_4Al_{18}Si_{7.5}O_{44}(OH)_4$

A symmetric solution model is used for Mg–Fe mixing in binary staurolite with the interaction parameter W(mst, fst) = −8·0 kJ/mol following White *et al.* (2001). End-members are:

Mg-staurolite (mst): $Mg_4Al_{18}Si_{7.5}O_{44}(OH)_4$;
Fe-staurolite (fst): $Fe_4Al_{18}Si_{7.5}O_{44}(OH)_4$.

Composition variables are x(st) = Fe/(Fe + Mg).

Downloaded from http://petrology.oxfordjournals.org/ at Indiana University School of Medicine Libraries on September 22, 2012

Phengitic muscovite (mu): $K\square^{M1}[Fe,Mg,Al]^{M2A}[Al]^{M2B}[Si,Al]_2^{T1}Si_2^{T2}O_{10}(OH)_2$

Following Coggon & Holland (2002), a non-ideal mixing model is used for the NCKFMASH phengitic muscovite where mixing between Al, Mg and Fe is assumed to occur only in the M2A site and mixing of tetrahedral Al and Si is restricted to the two T1sites. End-members are:

Muscovite (mu): $K\square\,{}^{M1}[Al]^{M2A}[Al]^{M2B}Al^{T1}Si^{T1}Si_2^{T2}O_{10}(OH)_2$;
Celadonite (cel): $K\square\,{}^{M1}[Mg]^{M2A}[Al]^{M2B}Si_2^{T1}Si_2^{T2}O_{10}(OH)_2$;
Fe–celadonite (fcel): $K\square\,{}^{M1}[Fe]^{M2A}[Al]^{M2B}Si_2^{T1}Si_2^{T2}O_{10}(OH)_2$;
Paragonite (pa): $Na\square\,{}^{M1}[Al]^{M2A}[Al]^{M2B}Al^{T1}Si^{T1}Si_2^{T2}O_{10}(OH)_2$.

Interaction parameters: W(mu, cel) = 0·2P kJ/mol, W(mu, fcel) = 0·2P kJ/mol, W(mu, pa) = (10·12 + 0·0054T + 0·353P) kJ/mol where the temperature coefficient was increased a little from the original 0·0034 after a series of test calculations, W(cel, fcel) = 0, W(cel, pa) = 52 kJ/mol and W(fcel, pa) = 52 kJ/mol. Composition variables: x(ph) = Fe/(Fe + Mg), y(ph) = x_{Al}^{M2A} and z(ph) = Na/(Na + K).

Biotite (bi): $K[Fe,Mg]_2^{M2}[Fe,Mg,Al]^{M1}[Si,Al]_2^{T1}Si_2^{T2}\,O_{10}(OH)_2$

Following Powell & Holland (1999), ordered biotite is modeled with symmetric mixing with Fe assumed to favor the M1 site. End-members are:

phlogopite (phl): $K[Mg]_2^{M2}[Mg]^{M1}Al^{T1}Si^{T1}Si_2^{T2}O_{10}(OH)_2$;
annite (ann): $K[Fe]_2^{M2}[Fe]^{M1}Al^{T1}Si^{T1}Si_2^{T2}O_{10}(OH)_2$;
eastonite (east): $K[Mg]_2^{M2}[Al]^{M1}Al_2^{T1}Si_2^{T2}O_{10}(OH)_2$;
ordered-biotite (obi): $K[Mg]_2^{M2}[Fe]^{M1}Al^{T1}Si^{T1}Si_2^{T2}O_{10}(OH)_2$.

Interaction parameters: W(phl, ann) = 9 kJ/mol, W(phl, east) = 10 kJ/mol, W(phl, obi) = 3 kJ/mol, W(ann, east) = −1 kJ/mol, W(ann, obi) = 6 kJ/mol, W(east, obi) = 10 kJ/mol, and a DQF parameter, $I_{obi} = -10·73$ kJ/mol.

Composition variables: x(bi) = Fe/(Fe + Mg), y(bi) = x_{Al}^{M1}, Q(bi) = $x_{Fe}^{M1} - x_{Fe}^{M2}$.

Jadeite (jd), omphacite (o) and diopsidic pyroxene (di): $[Ca,Na]^{M2}[Mg,Fe,Al]^{M1}Si_2O_6$

Following Holland & Powell (1996), the three pyroxenes are modeled with a same symmetric mixing and order–disorder model in which M1 and M2 sites are assumed to split into M1a, M1b, M2a and M2b, respectively, and the four end-members are:

jadeite (jd): $[Na]_{0·5}^{M2a}[Na]_{0·5}^{M2b}[Al]_{0·5}^{M1a}[Al]_{0·5}^{M1b}Si_2O_6$;
diopside (di): $[Ca]_{0·5}^{M2a}[Ca]_{0·5}^{M2b}[Mg]_{0·5}^{M1a}[Mg]_{0·5}^{M1b}Si_2O_6$;
hedenbergite (hed): $[Ca]_{0·5}^{M2a}[Ca]_{0·5}^{M2b}[Fe]_{0·5}^{M1a}[Fe]_{0·5}^{M1b}Si_2O_6$;
omphacite (om): $[Ca]_{0·5}^{M2a}[Na]_{0·5}^{M2b}[Mg]_{0·5}^{M1a}[Al]_{0·5}^{M1b}Si_2O_6$.

The interaction parameters are as follows: W(jd, di) = 26 kJ/mol, W(jd, hed) = 24 kJ/mol, W(jd, om) = 16 kJ/mol, W(di, hed) = 4 kJ/mol, W(di, om) = 16 kJ/mol and W(hed, om) = 17 kJ/mol and a DQF parameter $I_{om} = -3·5$ kJ/mol (Holland & Powell, 1996). The compositional variables are x(jd, o, di) = Fe/(Fe + Mg), J(jd, o, di) = $Al^{M1}/(Al + Mg + Fe)^{M1}$ and N(jd, o, di) = $(x_{Al}^{M1b} - x_{Al}^{M1a})/2$.

Glaucophane (gl): $[Na,Ca]_2[Mg,Fe]_3[Mg,Fe,Al]_2Si_8O_{22}(OH)_2$

Ideal mixing and DQF models are used for ternary glaucophane solution with three end-members:

glaucophane (gl): $Na_2Mg_3Al_2Si_8O_{22}(OH)_2$;
Fe-glaucophane (fgl): $Na_2Fe_3Al_2\,Si_8O_{22}(OH)_2$;
tremolite (tr): $Ca_2Mg_5Si_8O_{22}(OH)_2$.

The mixing between glaucophane and Fe-glaucophane is assumed to be ideal and the substitution of tremolite assumed to be non-ideal with a DQF parameter I_{tr} = 58 kJ/mol (Wei *et al.*, 2003). The composition variables are x(gl) = Fe/(Fe + Mg) and N(gl) = $[Na/(Na + Ca)]^{M4}$.

Paragonite (pa): $[Na,Ca]Al_3Si_3O_{10}(OH)_2$

A DQF model is used for Na–Ca mixing paragonite with I_{ma} = 12 kJ/mol (Vance & Holland, 1993). The end-members are:

paragonite (pa): $NaAl_3Si_3O_{10}(OH)_2$;
margarite (ma): $CaAl_4Si_2O_{10}(OH)_2$.
Compositional variable is c(pa) = Ca/(Ca + Na).

Plagioclase (pl): $[Na,Ca]\,[Al,Si]_4O_8$

A DQF model is used for Na–Ca mixing plagioclase with $I_{an} = (6·01 - 0·0035T + 0P)$ kJ/mol (Holland & Powell, 1992). The end-members are:

albite (ab): $NaAlSi_3O_8$;
anorthite (an): $CaAl_2Si_2O_8$.

Compositional variable is c(pl) = Ca/(Ca + Na).
Single end-member minerals with unit activities are:

zoisite (zo): $Ca_2Al_3Si_3O_{12}(OH)$;
lawsonite (law): $CaAl_2Si_2O_7(OH)_{2x}H_2O$;
kyanite (ky) and sillimanite (sill): Al_2SiO_5;
quartz (q) and coesite (coe): SiO_2.

Downloaded from http://petrology.oxfordjournals.org/ at Indiana University School of Medicine Libraries on September 22, 2012